University of Alberta

Numerical study of the crossover from free electrons to small polarons

by

Zhou Li

A thesis submitted to the Faculty of Graduate Studies and Research
in partial fulfillment of the requirements for the degree of

Doctor of Philosophy

Department of Physics

©Zhou Li
Fall 2012
Edmonton, Alberta

To

My father Jianmin Li and mother Yongxiang Wang

Abstract

The electron-phonon interaction is one of the fundamental interactions in almost all condensed matter materials. In conventional superconductors, the electron-phonon interaction is the glue that attracts two electrons to one another to form a pair. A strong electron-phonon interaction leads to the concept of a polaron, which is an electron with lattice distortions around it. The small polaron is a polaron with spatial extent comparable to an interatomic dimension of the solid. Evidence for polarons has been identified in many experiments in superconductors and semiconductors. In this thesis we present exact calculations of the polaron. Specifically we have refined Trugman's method to solve the ground state of an electron-phonon coupled system in the whole parameter regime, and we also generalized this method to treat spin-orbit coupled systems. The most difficult regimes, which is the strong-coupling regime and the small phonon frequency limit, have been solved by these refinements. There are three representative kinds of electron-phonon interaction, the Holstein model, the Fröhlich model and the BLF-SSH model. In this thesis we have addressed the first and the third one. The second one, the Fröhlich model, is very similar to the Holstein model but the interaction is nonlocal. For the Holstein model we have observed the expected smooth crossover from free electrons to small polarons, while for the BLF-SSH model, we have studied the weak coupling regime with perturbation theory and derived a new analytical result for the one-dimensional

problem.

Acknowledgements

Firstly, I would like to express my deep and sincere thanks to my supervisor and friend, Prof. Frank Marsiglio, for his talent in teaching and guiding me to conduct research in the area of condensed matter theory and more specifically, in the field of strongly correlated electrons. His tremendous support, both academically and financially, had made my PhD study at University of Alberta always exciting, and provided a lot of opportunities to attend international conferences, which is important for the development of my PhD projects.

I would also like to thank my committee members, Prof. Kevin Beach and Prof. Mark Freeman for their valuable suggestions and comments on my research proposal.

I would also like to thank my colleagues, Dr. Giang Bach, for discussions on dynamical mean field theory and the explanation of high temperature superconductivity, Dr. Fatih Dogan, for helping me to learn the techniques of Lanczos method, and Dr. Reza Nourafkan, for discussions on polaron physics and many body theory.

I would like to thank Dr. Lucian Covaci for sharing some results from Momentum Average method and valuable comments on the projects related to spin-orbit interaction.

I would also like to thank Joseph Ansong, Megumi, who had been my roommate for a long time and provided me a quiet and safe place to focus on my PhD study.

I would also thank Pastor Dennis at Church on 99 for his stimulating speeches on Sundays.

Contents

List of Tables

List of Figures

CHAPTER 1

Introduction

1.1 Superconductivity

A superconductor is one kind of material with zero resistivity and complete expulsion of magnetic field lines from the interior. The critical temperature of a superconductor is the temperature below which the material becomes superconducting. The first superconductor was Mercury, and was discovered by Heike Kamerlingh Onnes in Leiden in the year 1911. The critical temperature is about 4.2K. It then took a long time (about 46 years) for the theory of superconductivity to come out. In 1957, three American scientists J. Bardeen, L.N. Cooper and J.R. Schrieffer jointly developed the BCS theory for superconductivity. The key ingredient of this theory is that electrons can form Cooper pairs (Bardeen et al., 1957a,b), and the distance within one pair of two electrons can be very large, usually hundreds of times the lattice constant. The attraction to hold two electrons pairing together is from lattice phonons. No matter how weak the attraction is, there will be bound states. The attraction can be understood from the concept of the polaron. A polaron is an electron with lattice distortions (e.g. displaced positive ions) around it. Since the

electron moves much faster than the atoms, when it has already moved to another place, the ionic distortions are left behind. When another electron feels the attraction due to those positive ions, it comes into the center of the distortions. Thus these two electrons are attracting each other.

1.2 High temperature superconductivity

In 1986, K.A. Müller and J.G. Bednorz discovered superconductivity in the Cuprates, with a critical temperature of 35 K above absolute zero (Bednorz and Müller, 1986). They were awarded the Nobel Prize in 1987 and in their Nobel Prize lecture (Bednorz and Müller, 1988), they mentioned that they were stimulated by the idea that if an electron and a surrounding lattice distortion with a high effective mass can travel through the lattice as a whole, and a strong electron-lattice coupling exists then an insulator could become a high temperature superconductor. The conventional theory of superconductivity is greatly challenged because it seldom predicts such a high transition temperature. Many opinions (Mott, 1987; Anderson and Abrahams, 1987) were published for the explanation of high temperature superconductivity. For example, Anderson has pointed out that the resonating valence bond (RVB) theory could be the one (Anderson, 1987), Mott (Mott, 1987) has pointed out that Bose-Einstein condensation (BEC) of small bipolarons could be the one, and Hirsch (Hirsch, 2002) has pointed out the lowering of kinetic energy instead of the lowering of potential energy could be very important. The conventional theory of superconductivity consists of two distinct pieces. The first describes the formalism of pairing, premised on the idea that two electrons effectively attract one another; this pairing is well described by the Bardeen-Cooper-Schrieffer (BCS) wave function, (Bardeen et al., 1957a,b) and continues to be used extensively to describe almost all known

superconductors. The second piece concerns the origin of the attractive interaction, suggested originally by Fröhlich (Fröhlich, 1950) and Bardeen (Bardeen, 1950) to be the electron-phonon interaction, which is challenged by other sources of interaction such as the electron-electron interaction. In my opinion, the best scenario for high temperature superconductivity is probably a mixture of different interactions, for example, electron-phonon interaction plus some spin fluctuations.

1.3 Cold atoms

Recently Bose-Einstein condensation has been realized in cold atom experiments. In these experiments, the distance between two Fermions inside a Cooper pair can be tuned, from many lattice spacings (close to what happens for conventional BCS superconductors) to essentially on-site pairing (close to what happens for molecules to form a Bose-Einstein condensate). In this way, many interesting questions related to high temperature superconductivity could be answered and many idealized models (such as the Hubbard model (Hubbard, 1963, 1964), Holstein model (Holstein, 1959a,b)) can be directly tested. The experimental setup utilizes several laser beams(usually six, two in x-, two in y- and two in z- direction) traveling in opposite directions. By this way, a certain number of atoms can be trapped and their velocities can be systematically reduced. Combined with other cooling techniques (such as magnetic evaporative cooling (Anderson et al., 1995)), the temperature of the trapped atoms can be lowered down to a degree very close to absolute zero. At that time a new state of matter will emerge, in which a large fraction of the atoms will take the lowest quantum state of the external potential, giving us an example where quantum effects become apparent on a macroscopic scale. This kind of optical experiment was first realized in 1995 by Cornell, Wieman, and Wolfgang

Ketterle (Anderson et al., 1995; Davis et al., 1995), who were awarded the Nobel Prize in 2001. The above experiments all deal with bosons. The fermion condensate is more difficult to be realized because the Pauli principle prohibits fermions to occupy the same quantum state. However according to BCS theory, Cooper pairing of fermions can happen at very low temperature. The fermion superfluid will emerge and a fermion condensate is also possible. In 2003, Deborah Jin and collaborators at JILA managed to produce the fermion condensate for the first time (Greiner et al., 2003). In 2011, Lin et.al (Lin et al., 2011) showed that quantum many-body systems of ultracold atoms can be precisely controlled experimentally to provide an ideal platform on which to study spin-orbit coupling. Herrera et.al (Herrera and Krems, 2011) showed that an ensemble of polar molecules trapped in an optical lattice can be used to simulate the Holstein model.

1.4 Electron-phonon interaction

The electron-phonon interaction is the basic interaction in condensed matter physics, as almost all condensed matter materials consist of a lattice of atoms and electrons moving around them. At nonzero temperature, there are always some vibrations of the atoms. In classical mechanics, an arbitrary vibration can be decomposed into a sum of elementary vibrations called the normal modes (similar to Fourier analysis). In quantum mechanics, these normal modes are called phonons. Each phonon has a fixed energy and momentum. There are many effective models for the electron-phonon interaction problem, the representative three of which are the Holstein model (Holstein, 1959a,b), Fröhlich model (Fröhlich, 1950) and BLF-SSH (Barišić, Labbé, Friedel - Su, Schriffer, Heeger) model (Barišić et al., 1970; Barišić,

1972a,b; Su et al., 1979, 1980). The Holstein model is given by

$$H = -t \sum_{j,\delta} (c_j^\dagger c_{j+\delta} + c_{j+\delta}^\dagger c_j) \; - \; g\omega_E \sum_j c_j^\dagger c_j (a_j + a_j^\dagger) + \omega_E \sum_j a_j^\dagger a_j, \qquad (1.1)$$

where $c_j^\dagger, c_j$ are creation and annihilation operator of an electron at site j, $a_j^\dagger, a_j$ are creation and annihilation operator of a phonon at site j, ω_E is the frequency of the phonon and g is the strength of electron-phonon interaction. The commutation and anticommutation relations of these operators are $[a_i, a_j^\dagger] = \delta_{i,j}, [a_i, a_j] = 0, [a_i^\dagger, a_j^\dagger] = 0$ and $\{c_i, c_j^\dagger\} = \delta_{i,j}, \{c_i, c_j\} = 0, \{c_i^\dagger, c_j^\dagger\} = 0$, respectively. There are three parts of the hamiltonian. The first is the kinetic energy of the electron, described by the tight binding approximation, which is an approximate approach to calculate the band structure from a superposition of electronic wave functions at each atomic site. The kinetic energy is characterized by the parameter t, which is a measure of the probability for an electron to hop between neighboring sites. It is determined by the overlap integral of the electronic wave functions at each atomic site. The second part is the electron-phonon interaction; for the Holstein model, the electron couples to optical phonons, and the interaction is local as the ionic distortion will only affect the electron energy level at a specific site. The third part is the total energy of phonons represented by a sum over the number of phonons at each site. For the Fröhlich model, the electron also couples to optical phonons, but the electron-phonon interaction is nonlocal as the ionic distortion will affect the electron energy level at many sites. For the BLF-SSH model, which is shown in chapter 5, the electron couples to acoustic phonons instead of optical phonons, and the electron-phonon interaction will modify the hopping amplitude instead of electron energy level. This is due to the fact that when atoms are vibrating, the overlap of electronic wave functions is also changing.

In all these three models, there is a weak coupling regime and a strong coupling regime. The weak coupling regime refers to the case where the electron-phonon interaction is small compared to the kinetic energy of electron. So the problem can be solved by perturbation theory. Usually a first order expansion is good enough to get converged results of the ground state properties. The strong coupling regime refers to large electron-phonon interaction. In this regime one need to sum up an infinite number of Feynman diagrams, each diagram corresponding to a term in the perturbation expansion. This task is usually impossible, so a non-perturbative method is required, although for very strong electron-phonon interaction and certain models (e.g. Holstein model), one can use the Lang-Firsov (Lang and Firsov, 1963) transformation to map the strong coupling problem into a weak coupling problem and solve it by perturbation theory. In the calculation of Feynman diagrams one may meet the problem of artificial divergence caused by the integration near zero momentum (named the infrared divergence). By setting the problem on a lattice, this artificial divergence will be naturally removed, so the divergence we have obtained will have its physical meaning, e.g. the divergence of the effective mass. We have developed a refined Lanczos method for both regimes, the details are described in the following section. In the weak coupling regime, the distance between two electrons inside a Cooper pair will be very large, similar to what is described in the BCS theory. In the strong coupling regime, the distance between two electrons inside a Cooper pair will be very small, similar as what happens for the BEC of small bipolarons. The crossover, from the weak coupling regime to the strong coupling regime, is of quite interest, because in a lot of real materials the strength of the electron phonon interaction is intermediate. The intermediate regime is difficult for numerical simulations because the number of states that need to be retained in the Hilbert space is very large.

When the spin degree of freedom of the electron is considered, there remains the possibility of other interactions. In the following chapters, we will consider the spin-orbit interaction, which is the coupling of the electron's spin with its motion. This interaction will cause the spin to flip while the electron is hopping on the lattice sites. The spin-orbit interaction is found to be prominent in two dimensional systems that lack inversion symmetry, and plays the key role in the field of spintronics. There are two kinds of spin-orbit interaction described by Rashba (1960) and Dresselhaus (1955). The ground state will be dramatically changed by these spin-orbit interactions; the momentum of the ground state will be shifted from zero to nonzero, the degeneracy of the ground state will jump from one to four (for one spin-orbit interaction, either Rashba or linear Dresseulhaus) or two (for the coexistence of Rashba and linear Dresseulhaus spin-orbit interaction). Thus the ground state properties (e.g. ground state energy, effective mass) of a single polaron can be tuned by spin-orbit interactions. In Chapter 3 and 4 we will discuss these effects in detail.

1.5   Lanczos method

The Lanczos method is a general method (Fehske and Trugman, 2007; Dagotto, 1994; Haydock et al., 1972, 1975) to transform a sparse $N \times N$ matrix into a smaller tridiagonal $M \times M$ matrix. N is the number of states in the subspace of the infinite Hilbert space. $M \leq N$ should be satisfied, although good convergence may be achieved for M much smaller than N. By choosing an initial random N-dimensional state $|\phi_0\rangle$, and then applying the Hamiltonian H on it, we can generate the Krylov subspace $(|\phi_0\rangle, H|\phi_0\rangle, H^2|\phi_0\rangle, H^3|\phi_0\rangle......)$. To construct orthogonal basis

states spanning the Krylov subspace, we use the following steps:(Dagotto, 1994)

$$|\phi_1\rangle = H|\phi_0\rangle - \frac{\langle\phi_0|H|\phi_0\rangle}{\langle\phi_0|\phi_0\rangle}|\phi_0\rangle \tag{1.2}$$

$$|\phi_2\rangle = H|\phi_1\rangle - \frac{\langle\phi_1|H|\phi_1\rangle}{\langle\phi_1|\phi_1\rangle}|\phi_1\rangle - \frac{\langle\phi_1|\phi_1\rangle}{\langle\phi_0|\phi_0\rangle}|\phi_0\rangle \tag{1.3}$$

And more generally

$$|\phi_{n+1}\rangle = H|\phi_n\rangle - a_n|\phi_n\rangle - b_n^2|\phi_{n-1}\rangle \tag{1.4}$$

where $a_n = \frac{\langle\phi_n|H|\phi_n\rangle}{\langle\phi_n|\phi_n\rangle}, b_n^2 = \frac{\langle\phi_n|\phi_n\rangle}{\langle\phi_{n-1}|\phi_{n-1}\rangle}, n = 0, 1, 2...$The basis states are orthogonal to each other, $\langle\phi_i|\phi_j\rangle = 0$, for $i \neq j$. In practice, due to the numerical error of the computer, these states may lose orthogonality after a large number of iterations and one need to perform a re-orthogonalization of the Krylov vectors. This re-orthogonalization technique is used when one is interested in the excited states; for the ground state, the re-orthogonalization is not needed. In this basis, the Hamiltonian matrix becomes

$$H = \begin{bmatrix} a_0 & b_1 & 0 & 0 & ... \\ b_1 & a_1 & b_2 & 0 & ... \\ 0 & b_2 & a_2 & b_3 & ... \\ 0 & 0 & b_3 & a_3 & ... \\ ... & ... & ... & ... & ... \end{bmatrix}. \tag{1.5}$$

For example, to calculate the diagonal matrix elements, we have, $H_{nn} = \frac{\langle\phi_n|H|\phi_n\rangle}{\sqrt{\langle\phi_n|\phi_n\rangle}\sqrt{\langle\phi_n|\phi_n\rangle}} = a_n$. To calculate the nondiagonal elements, we have $H_{n-1,n} = \frac{\langle\phi_{n-1}|H|\phi_n\rangle}{\sqrt{\langle\phi_{n-1}|\phi_{n-1}\rangle}\sqrt{\langle\phi_n|\phi_n\rangle}} = \frac{\langle\phi_n|\phi_n\rangle}{\sqrt{\langle\phi_{n-1}|\phi_{n-1}\rangle}\sqrt{\langle\phi_n|\phi_n\rangle}} = \sqrt{\frac{\langle\phi_n|\phi_n\rangle}{\langle\phi_{n-1}|\phi_{n-1}\rangle}} = b_n$. Now the matrix is tridiagonal and can be easily diagonalized by standard routines.

To show how the basis states are generated for electron-phonon coupled systems, we consider the Holstein model. If we choose the initial state to be a Bloch state with translational symmetry, that is

$$|\phi_0\rangle = \sum_j e^{ikR_j} c_j^\dagger |0\rangle \tag{1.6}$$

and then apply the Hamiltonian to this state; we get

$$
\begin{aligned}
H|\phi_0\rangle &= -t \sum_j e^{ikR_j}(c_{j+1}^\dagger + c_{j-1}^\dagger)|0\rangle - g\omega_E \sum_j e^{ikR_j} c_j^\dagger a_j^\dagger |0\rangle \\
&= -2t\cos k \sum_j e^{ikR_j} c_j^\dagger |0\rangle - g\omega_E \sum_j e^{ikR_j} c_j^\dagger a_j^\dagger |0\rangle
\end{aligned} \tag{1.7}
$$

Now the Hilbert space includes a new state with one electron and one phonon on the same site. By applying the Hamiltonian to $|\phi_0\rangle$ many times, we generate the Krylov subspace with many phonons. Since phonons are bosons, the Hilbert space will be infinite; especially for strong coupling ($g\omega_E >> t$), the phonon number will be very large and it seems impossible to get converged results for the ground state energy. We have developed a numerical routine to search the Hilbert space automatically. After several iterations, the numerical routine will converge to the ground state energy for a certain set of parameters, then one parameter is changed by a small amount and the same procedure is applied to the new parameter set until convergence is achieved. By this we can get converged results for the entire parameter regime. We have observed that in the intermediate coupling regime ($g\omega_E \simeq t$) or near the adiabatic limit ($\omega_E << t$), the number of states to be retained in the Hilbert space will be very large and it take more iterations to get convergence.

Once the ground state is known, we can also calculate the spectral properties (e.g.

spectral function, optical conductivity) by the Lanczos method. Although the results of these calculations are not included in this thesis, we nonetheless include the details of the calculations in an appendix.

1.6 Outline of the following chapters

In Chapter 2, we will discuss the refined Lanczos method to calculate the ground state properties of the Holstein model near the adiabatic limit. At strong coupling, the refinement leads to a rapid convergence of results. The intermediate coupling regime is further handled with an adaptive algorithm. We also use semiclassically derived results for the adiabatic end-point, along with weak coupling perturbation theory. These establish weak and strong coupling (or large and small polaron, respectively) regimes in two dimensions or higher.

In Chapter 3, we apply the refined Lanczos method to calculate the ground state properties of a polaron in the presence of a Rashba spin orbit coupling. Our results corroborate with previous work performed with the Momentum Average approximation and with weak coupling perturbation theory. We find that spin orbit coupling increases the effective mass in the regime with weak electron phonon coupling, and decreases the effective mass in the intermediate and strong electron phonon coupling regime. Analytical strong coupling perturbation theory results confirm our numerical results in the small polaron regime. A large amount of spin orbit coupling can lead to a significant lowering of the polaron effective mass.

In Chapter 4, we apply the refined Lanczos method to calculate the ground state properties of a polaron in the presence of a Rashba and linear Dresselhaus spin-orbit coupling. We find that when the linear Dresselhaus spin-orbit coupling approaches the Rashba spin-orbit coupling, the Van-Hove singularity in the density of states will

be shifted away from the bottom of the band and finally disappear when the two spin-orbit couplings are tuned to be equal. The effective mass will be suppressed; the trend will become more significant for low phonon frequency. The presence of two dominant spin-orbit couplings will make it possible to tune the effective mass with more varied observables.

In Chapter 5, we study the BLF-SSH model using both a perturbative Green's function analysis and standard perturbative quantum mechanics to calculate the decrease in energy and the effective mass for an electron interacting with acoustic phonons. The interaction is between the difference in lattice displacements for neighbouring ions, and the hopping amplitude for an electron between those two sites. The calculations are performed in one, two, and three dimensions, and comparisons are made with other electron-phonon models. We also compute the spectral function and quasiparticle residue, as a function of characteristic phonon frequency, and make comparisons with other models. There are strong indications that this model is always polaronic for one dimension, where an unusual relation between the effective mass and the quasiparticle residue is also found.

CHAPTER 2

Holstein Polaron [1]

2.1 Introduction

There has been considerable work performed over the last two decades on the Holstein model (Holstein, 1959a,b). Interest in this model is fueled by the fact that it serves as the paradigm for electron-phonon interactions, much like the Hubbard model (Hubbard, 1963, 1964) serves the same purpose for electron-electron interactions. While a considerable amount of this work has focussed on the many-electron problem, another subset has examined the single-electron, or polaron problem (Fehske and Trugman, 2007; Alexandrov, 2007). Among all the numerical techniques for determining polaron properties in the thermodynamic limit, the variational procedure outlined by Trugman and coworkers (Trugman, 1990; Bonča et al., 1999) proves to be a very powerful and general method. With this method properties such as the ground state energy and the effective mass are readily obtained, in any dimension, over almost all parameter regimes. One range of parameter space that has remained difficult, however, is near the adiabatic limit, which is what we

---

[1]A version of this chapter has been published. Zhou Li et.al, 2010, Phys. Rev. B 81, 115114.

address in this chapter. The actual adiabatic limit was first treated by Kabanov and Mashtakov (Kabanov and Mashtakov, 1993); they found that in one dimension (1D), the electron retains polaronic character for all electron-phonon coupling strengths, while in two dimensions and higher there is a critical coupling strength, below which the electron behaves in a free-electron-like manner, and above which it is polaronic. At the same time, away from the adiabatic limit the problem is known from numerical solutions to have a smooth crossover as a function of coupling strength (i.e. no abrupt transition), so it is of interest to pursue this crossover as the phonon frequency decreases towards zero. This was done to some degree in one dimension (Alexandrov et al., 1994; Marsiglio, 1995), but only for rather small lattices. Our aim is to examine this limit using the Trugman variational technique (Bonča et al., 1999; Ku et al., 2002). In the next section we outline the model, and establish notation, etc. In Section 2.3 we describe some refinements to the variational method, and provide some illustrative examples to demonstrate the improvement in convergence. In Section 2.4 we provide some numerical results as the adiabatic parameter ω_E/t approaches zero. Also provided are some perturbation theory results, which can be reinterpreted to provide constraints for the numerical results. In Section 2.5 we show some results concerning the expected numbers of phonons in the ground state, which gives another indication of the difficulty of the adiabatic limit. In Section 2.6 we show some results in 3D.

2.2 The model

The model that most simply describes an electron interacting with optical phonons is the Holstein Hamiltonian, given by

$$H = -t \sum_{i,\delta} (c_i^\dagger c_{i+\delta} + c_{i+\delta}^\dagger c_i) \ - \alpha \sum_i n_i x_i + \sum_i (\frac{p_i^2}{2M} + \frac{1}{2} M \omega_E^2 x_i^2), \qquad (2.1)$$

which is also written as the Eq. (1.1) in chapter 1. The ion momentum p_i, and displacement x_i are quantized via

$$x_i = \sqrt{\frac{1}{2M\omega_E}} (a_i^\dagger + a_i)$$

$$p_i = i \sqrt{\frac{M\omega_E}{2}} (a_i^\dagger - a_i)$$

where M is the ion mass (we set $\hbar = 1$) and $a_i^\dagger$ (a_i) creates (annihilates) a phonon at site i. The sum over i is over all sites in the lattice, whereas the sum over δ is over nearest neighbors. Here, as the notation already makes clear, we confine ourselves to nearest neighbor hopping only. The parameters are the hopping integral t, the phonon frequency ω_E, and the coupling of the electron to the oscillator degrees of freedom, α. This parameter is the bare coupling between the electron and the ion; however, it is rarely used, and instead in the polaron literature the dimensionless coupling constant $g = \frac{1}{\omega_E} \frac{\alpha}{\sqrt{2M\omega_E}}$ is used. In the many-body literature, the dimensionless parameter $\lambda \equiv 2g^2 \omega_E / W$ is used, where $W \equiv 2zt$ is the electronic bandwidth for a cubic tight-binding model with coordination number z ($z = 2, 4, 6$ in $1, 2, 3$ dimensions, respectively). In two dimensions it is arguably more useful to use $\lambda \equiv 2g^2 \omega_E / (4\pi t)$, where $1/(4\pi t)$ is the value of the non-interacting electron density of states at the bottom of the band (as opposed to the average density of

states). The parameter λ has historical significance for the effective mass of degenerate electrons weakly coupled to phonons. Alternatively, and most useful in the strong coupling regime, the parameter g (or g^2) can be used to characterize the coupling strength. It appears in the Lang-Firsov transformation (Lang and Firsov, 1963), and leads to a band narrowing factor $t \rightarrow t^* = te^{-g^2}$ in first order degenerate perturbation theory.

As mentioned in the introduction this model has been most successfully analyzed using a refinement of the standard Lanczos method due to Trugman (Trugman, 1990; Bonča et al., 1999). Very accurate results can be obtained in any dimension (Ku et al., 2002) in almost all parameter regimes (Bonča et al., 1999; Ku et al., 2002; Fehske and Trugman, 2007). A difficulty remains for moderately to strongly coupled systems with low adiabaticity parameter ω_E/t. For example, if one uses the Lang-Firsov transformation (Lang and Firsov, 1963) to define the zeroth order strongly coupled wave function, then the average number of phonons in the ground state can be readily determined to be approximately g^2. For typical parameters in the moderately coupled regime (in one dimension), say $\omega_E = 0.05t$, and $\lambda = 1.0$, then $g^2 = 40$, and this is the approximate number of phonons in the ground state. The Trugman procedure starts with a bare electron; on a moderate work station a feasible number of applications of the Hamiltonian is $N_h = 22$ (Bonča et al., 1999), which produces a Hilbert space of order 10^7. This process with $N_h = 22$ produces states that contain a maximum of 22 phonons, and cannot possibly yield the correct ground state.

2.3 Refinement of the Trugman method

We have examined two simple refinements to the Trugman method (Trugman, 1990; Bonča et al., 1999); instead of starting with the bare electron state (properly extended throughout an infinite lattice), we first start with the state which is used as the unperturbed state in the strong-coupling limit (Lang and Firsov, 1963; Marsiglio, 1995):

$$|\psi> = e^{-g^2/2} \sum_\ell e^{ikR_i} e^{-g\hat{a}_\ell^\dagger} \hat{c}_\ell^\dagger |0>, \qquad (2.2)$$

where the sum is over all lattice sites. As we shall see in what follows this speeds up convergence considerably in the strong coupling regime (either $\lambda >> 1$ or $\omega_E << t$). An example of the increased convergence is illustrated in Fig. 2.1. Following Fig. 2 of Ku et al. (2002) we show the fractional error Δ as a function of the number of states kept in the Hilbert space, for two sets of parameters, both of which have $g^2 = 20$, using the bare electron as the starting state and using the strong-coupling solution as the starting state. There is a clear numerical advantage to using the latter. In Fig. 2.1(c) we show the fractional error for a parameter regime near $\lambda \approx 1$, where the strong coupling start is better even for values of $\lambda < 1$. It is also clear that as λ increases beyond the range of this figure, the refinement becomes increasingly useful.

In pursuit of more severely disparate electron and phonon energy scales we found that even starting with the strong coupling solution resulted in slow convergence when λ was of order unity. A remedy to this difficulty is the following procedure: start at large values of λ, where convergence is readily obtained after a few iterations. Lower the value of λ by a small amount, and use as a starting wave function the previous solution, truncated to include components with some minimal amplitude
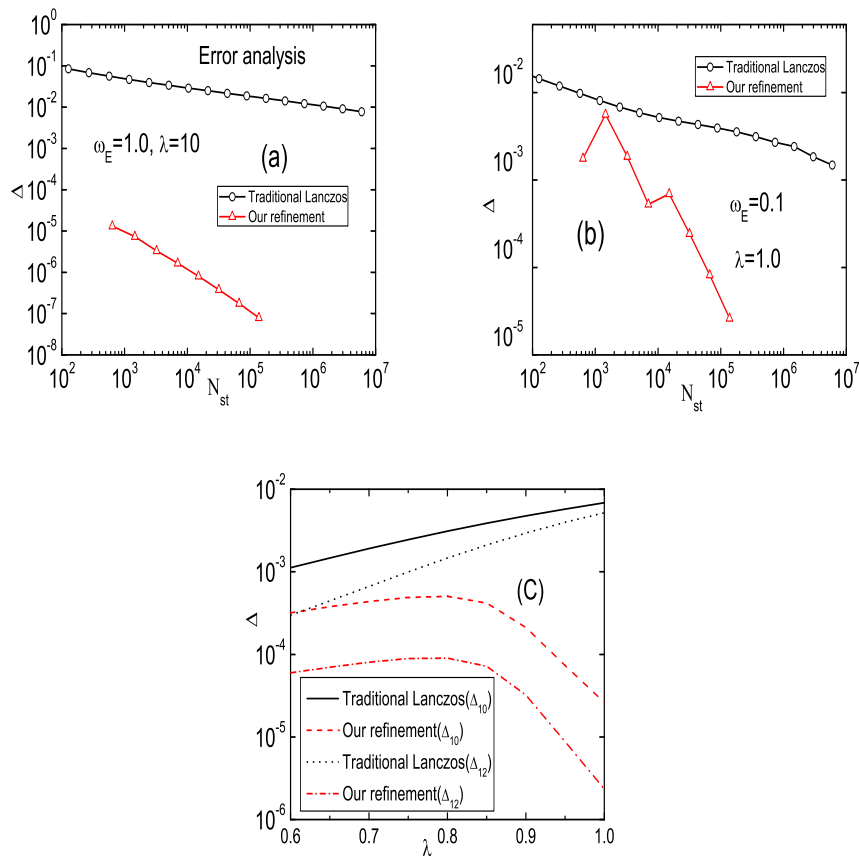
Figure 2.1: Fractional error vs. number of states for (a) a very strong coupling case, and (b) a moderate coupling, but with $\omega_E/t = 0.1$. In both cases our refinement speeds up convergence considerably. In (c) we show the improvement over a range of coupling strength near $\lambda = 1$; for $\lambda > 1$ (not shown) it is clear that the refinement leads to much better convergence. Note that the fractional error does not have to decrease monotonically with the number of states added.

(so that a few hundred basis states at most are used). Then converge the solution for this value of λ, lower it, and continue the process until the desired range is covered. We have found this latter procedure to be the most robust, particularly when the phonon frequency is much smaller than the electron hopping parameter, t.

In Fig. 2.2 we show the ground state energy E_0 vs. λ for various values of the phonon frequency; this is in one dimension. Fig. 2.3 shows similar results in two dimensions. It is clear that as the phonon frequency decreases, the crossover region near $\lambda \approx 1$ (actually, the critical value of λ, only valid in the adiabatic limit, is closer to 0.55) becomes sharper. This is consistent with the result that, in the adiabatic limit, there is a transition from a small polaron state to a free electron-like state, in dimensions two and higher (Kabanov and Mashtakov, 1993). Nonetheless, as is known through other considerations (Löwen, 1988), for any non-zero phonon frequency, the crossover is smooth.

To summarize this section, we have obtained numerically exact results for a wide range of parameters, by using refinements to the method used in Trugman (1990) and Bonča et al. (1999). In particular, we obtain well converged results over all coupling strengths *and* for low phonon frequencies, $\omega_E << t$. The results for low frequencies in particular illustrate a rather abrupt crossover to a regime where multi-phonon processes are prevalent. To what extent they play a crucial role even at intermediate coupling strengths is the subject of the next section.

2.4   Perturbation theory

Perturbation theory can be performed both from the weak and the strong coupling limits. In Marsiglio (1995) he obtained, to second order (in g), in one dimension,
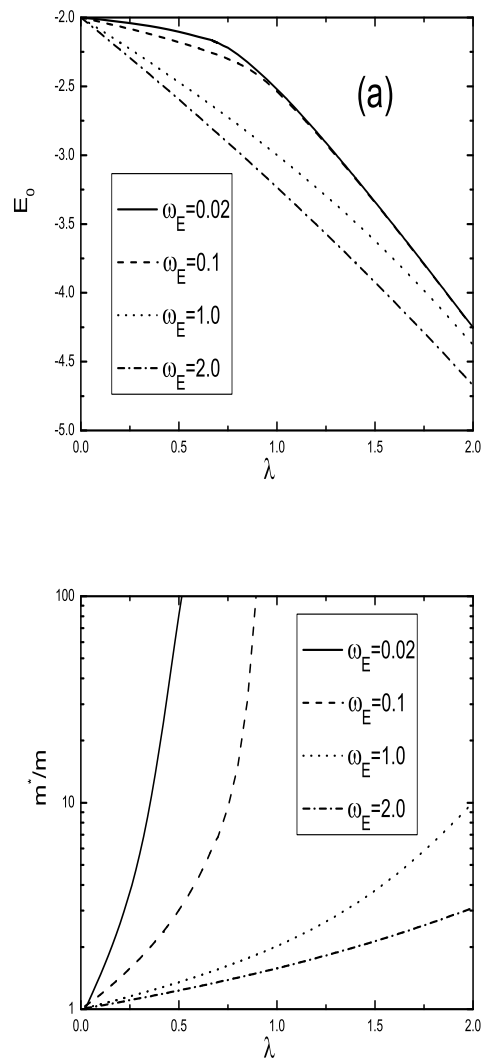
Figure 2.2: Ground state energy E_0 vs. λ and m*/m vs. λ for various phonon frequencies, in one dimension. There really is no special value of λ singled out in these curves, consistent with the crossover phenomenon discussed in the text.
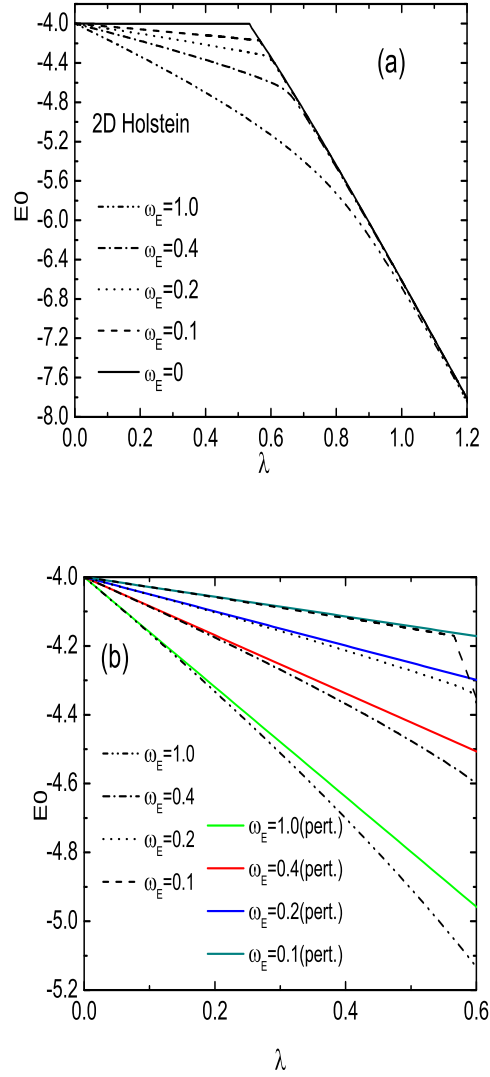
Figure 2.3: Ground state energy E_0 vs. λ for various phonon frequencies, in two dimensions. In contrast to the 1D results in Fig. 2.2, a special value of λ is now apparent $\lambda \approx 0.55$. However, for any non-zero phonon frequency the behaviour below and above this special value is smoothly connected. Only in the adiabatic limit does the behaviour change abruptly. (b) Expansion of the weak coupling regime showing the numerical results along side the perturbation theory results. Agreement is very good.
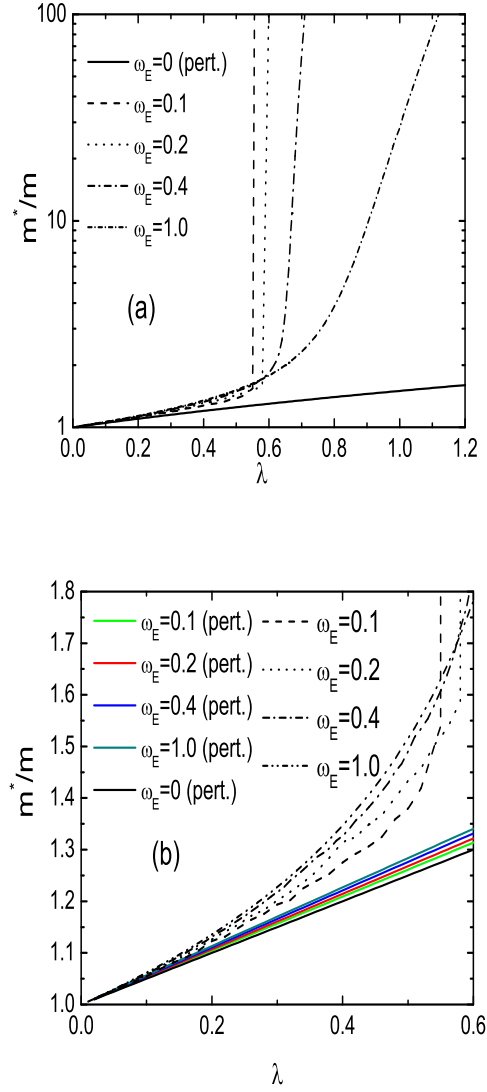
Figure 2.4: Effective mass m*/m vs. λ for various phonon frequencies, in two dimensions. Again, unlike the results in 1D in Fig. 2.2, a special value of λ is clear $\lambda \approx 0.55$. However, for any non-zero phonon frequency the behaviour below and above this special value is smoothly connected. Only in the adiabatic limit does the behaviour change abruptly. (b) Expansion of the weak coupling regime showing the numerical results alongside the perturbation theory results. Agreement is not as good as in Fig. 2.3.

the self energy

$$\Sigma_{1D}(\omega + i\delta) = \frac{\lambda \omega_E \text{sgn}(\omega - \omega_E)}{\sqrt{\left(\frac{\omega - \omega_E}{2t}\right)^2 - 1}};$$

(2.3)

which leads to a ground state energy:

$$E_0 = -2t\left(1 + \lambda\sqrt{\frac{\omega_E}{4t + \omega_E}}\right).$$

(2.4)

This expression is somewhat misleading; for very large frequency $\omega_E >> t$ there is a correction by a factor $1 + \lambda$ reminiscent of the mass renormalization for the electron mass in a Fermi liquid state. On the other hand, as the frequency becomes small the first order correction vanishes. In fact the most significant effect of the phonon coupling to a single electron occurs for low phonon frequencies, while the effect disappears for high phonon frequency. This is most readily seen by examining the quasiparticle residue z_0

$$z_0 = 1 - \frac{\lambda}{2}\sqrt{\frac{t}{\omega_E}}\frac{1 + \frac{\omega_E}{2t}}{(1 + \frac{\omega_E}{4t})^{3/2}}.$$

(2.5)

or the effective mass, defined as

$$m/m^* = \frac{1}{2t}\frac{\partial^2 E(k)}{\partial k^2}|_{k=0}.$$

(2.6)

For a momentum independent self energy (as in the second order weak coupling expansion) these are simply related: $m^*/m = 1/z_0$. The residue clearly approaches the non-interacting value, unity, as $\omega_E \to \infty$, while it diverges as $\omega_E \to 0$. This indicates a breakdown in (weak coupling) perturbation theory in this limit, which is consistent with the fact that the electron is polaron-like for all coupling strengths, i.e. there is an abrupt change in character only at g = 0. In fact, as established

in Holstein (1959a,b) for a two-site model, and in Kabanov and Mashtakov (1993), the effective mass diverges in the adiabatic limit for all coupling strengths (in 1D), a limit which we now approach numerically in Fig. 2.2(b).

In two dimensions (2D), we use $\lambda = g^2 \omega_E/(2\pi t)$. This actually uses the electron density of states at the bottom of the band, $N(0) = 1/(4\pi t)$, instead of the average density of states that is commonly used, $N_{\text{ave}}(0) = 1/(8t)$. The reason for this choice is that we are studying the one electron sector, so the most pertinent density of states is the one at the bottom.

The self energy in 2D in weak coupling is given by

$$\Sigma_{2D}(\omega + i\delta) = \frac{\lambda}{2} \frac{8t\omega_E}{\omega - \omega_E} K\left[\left(\frac{4t}{\omega - \omega_E} \right)^2 \right],$$

(2.7)

where $K(x) \equiv \int_0^{\pi/2} d\theta \frac{1}{\sqrt{1 - x \sin^2 \theta}}$ is the complete Elliptic integral of the first kind. This leads to a ground state energy, which, in weak coupling, is:

$$E_0 = -4t \left(1 + \frac{\lambda}{4} \frac{\omega_E}{t} \frac{1}{1 + \omega_E/(4t)} K\left[\frac{1}{\left(1 + \omega_E/(4t) \right)^2} \right] \right).$$

(2.8)

We can take the derivative of Eq. (2.7) to obtain:

$$m^*/m = 1 + \frac{\lambda}{2} \frac{1}{1 + \omega_E/(8t)} E\left[1/(1 + \omega_E/(4t))^2 \right],$$

(2.9)

where $E(x) \equiv \int_0^{\pi/2} d\theta \sqrt{1 - x \sin^2 \theta}$ is the complete Elliptic integral of the second kind. We have used, $\frac{\partial K(x)}{\partial x} = \frac{1}{2x} \left(\frac{E(x)}{1-x} - K(x) \right)$. All of these calculations are done using perturbation theory; i.e. the self energy is evaluated non self-consistently.

More familiar expressions are available, for cases when the arguments of the complete elliptic integrals are close to unity. This occurs for $\omega_E << t$. Using $\lim_{m \to 1} K(m) =$

$\frac{1}{2}\ln(16/m_1)$, where $m_1 = 1 - m$, an approximate form for the ground state energy is:

$$E_0 \approx -4t\left(1 + \frac{\lambda}{4}\frac{\omega_E}{t}\frac{1}{1 + \omega_E/(4t)}\ln\left[4\sqrt{\frac{2t}{\omega_E}}\frac{1 + \omega_E/(4t)}{\sqrt{1 + \omega_E/(8t)}}\right]\right). \qquad (2.10)$$

From Eq. (2.9) we obtain:

$$m^*/m = 1 + \frac{\lambda}{2} + \lambda\frac{\omega_E}{16t}\ln\left(\frac{32t}{\omega_E}\right) + O\left(\left(\frac{\omega_E}{t}\right)^2\ln\left(\frac{t}{\omega_E}\right)\right). \qquad (2.11)$$

Note that as $\omega_E/t \to 0$, this result approaches the one derived in the continuum limit by Cappelluti et al. (Cappelluti et al., 2007a), and the mass enhancement is half that expected when E_F is large.

In Fig. 2.3a, we show the ground state energy of the 2D Holstein model as a function of λ for a variety of phonon frequencies; we also show the result in the adiabatic limit as $\omega_E/t \to 0$. For the latter case, we adopted the iterative method described in Kabanov and Mashtakov (1993) and Marsiglio (1995), and used Lanczos diagonalization for the electronic portion. The abrupt transition occurs because we do not assume Bloch's theorem, and translational invariance is broken for sufficiently strong coupling. For non-zero phonon frequency we note the trend that as $\omega_E/t \to 0$, the crossover from free-electron-like behaviour to polaronic behaviour becomes more abrupt, though it is always smooth.

In Fig. 2.3b we show an expanded region in the weak coupling regime, where the perturbation theory results are also plotted. Note that they are quite accurate for all frequencies shown.

In Fig. 2.4a, we show the electron effective mass for the same parameters as in Fig. 2.3. In strong coupling the effective mass grows rapidly with coupling strength, as shown. However, this increase is even more pronounced as the phonon frequency de-

creases, until, as the adiabatic limit is approached, the increase becomes very nearly abrupt above a critical coupling strength, as determined through the adiabatic calculation. At weak coupling, the effective mass is unity for large ω_E (not shown). As the phonon frequency decreases, the effective mass grows; however, for smaller phonon frequencies the effective mass will decrease again as the phonon frequency decreases (as can be seen from the cases shown). Both of these trends conspire to make the crossover more abrupt as the phonon frequency approaches zero.

In Fig. 2.4b we show an expanded region in the weak coupling regime (no log scale), where the perturbation theory results are also plotted. The results are certainly not as accurate as the ground state energy; however, the inversion with phonon frequency noted above is clearly obtained.

2.5   Mean phonon numbers

We briefly examine the expectation of the number of phonons in the ground state, and the impact on the electronic dispersion relation. Restricting ourselves to two dimensions, we plot, in Fig. 2.5a, the mean phonon number vs. coupling strength in the intermediate coupling regime for several phonon frequencies. The same trend as seen in Fig. 2.4 is apparent beyond a special coupling strength the mean phonon number grows very abruptly from near zero to some value, N_c after which it continues to grow gradually as the coupling strength increases. The actual value of N_c is close to the central value of the Poisson distribution as predicted by strong coupling perturbation theory. In Fig. 2.5b, we shows numerical results of the mean phonon number as a function of total momentum k_x, of the electron-phonon system, for a few values of phonon frequency, and for a very low value of coupling (so that the results are well converged). Despite this small value of coupling, convergence is
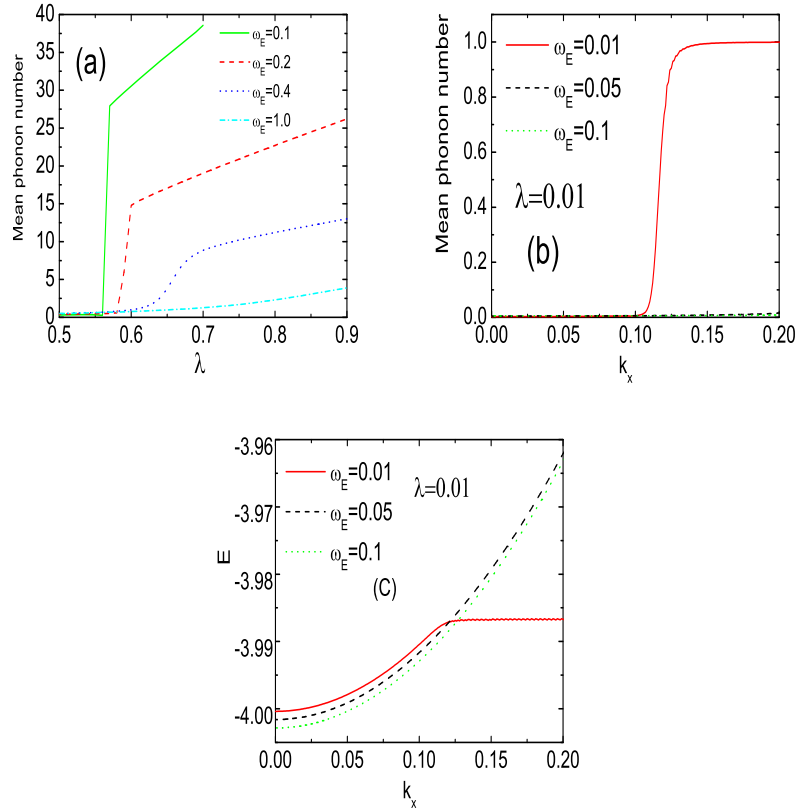
Figure 2.5: (a) Mean phonon number vs. coupling strength for various phonon frequencies (in 2D). Note the increasingly abrupt behaviour as the phonon frequency decreases. (b) Mean phonon number as a function of wave vector. Even for very small coupling strength there is an abrupt increase when the phonon frequency is small enough. Explanation is provided in the text, and is confirmed by (c) where the energy as a function of wave vector is plotted for the same parameters as in (b).

difficult because we use ω_E as small as 0.01t. We apply our self-adaptive Lanczos method by first converging the results for some high momentum (say, $k_x = 0.3$ we keep $k_y = 0$), and then lower the value of k_x in small increments, and converge the calculation at each step, until we finally reach the desired end-point ($k_x = 0$). As Fig. 2.5b illustrates, for sufficiently small phonon frequency, the mean phonon number shows a sharp increase from close to zero to nearly unity at some wave-vector, say k_c. The reason for this is that the energy difference with the ground state will eventually exceed a value of order ω_E; at this point it becomes energetically more favorable to use the zero momentum state (with much lower energy), and simply excite a phonon with the required momentum. Confirmation of this explanation is provided in Fig. 2.5c, where the dispersion flattens abruptly beyond k_c, when the energy exceeds that of the ground state by an amount approximately equal to ω_E. It retains this value because phonon momenta of any value are available with the same energy.

2.6 Results in 3D

Results are summarized in Fig. 2.6 for the one dimensional (a) and (b), two dimensional (c) and (d), and three dimensional (e) and (f) ground state energy and effective mass, respectively, vs. electron phonon coupling strength, for a variety of phonon frequencies. The main results can be summarized as follows: in 1D the electron is *always* polaron-like. Note in particular that as the phonon frequency decreases the effective mass increases dramatically (Fig. 2.6b), and essentially diverges in the adiabatic limit, even for infinitesimal coupling strength. The results for the ground state go smoothly over to the adiabatic limit, as is apparent from the disappearance of two of the finite frequency curves into the adiabatic curve in

Fig. 2.6a. In 2D and 3D there are clear delineations of free electron-like behaviour at weak coupling and polaron-like behaviour at intermediate and strong coupling. However all the results are 'smooth' for a non-zero phonon frequency — only when an adiabatic calculation is performed (with the phonon frequency set equal to zero at the onset) does the curve display a kink (and therefore a transition). So no phase transition occurs as long as $\omega_E \neq 0$. The remarkable result is that the crossover to polaron-like behaviour occurs at such an intermediate coupling strength (Alexandrov and Mott, 1995), well below the value of coupling strength normally assigned to conventional superconductors (even in 2D, if the average electronic density of states is used in the definition of λ, the crossover coupling strength only moves up to about 0.86, just a little lower than the value in 3D).

2.7   Chapter Summary

We have implemented an adaptation to the variational method first suggested by Trugman, specifically to handle the adiabatic regime. In strong coupling our starting point leads to immediate convergence, while in the intermediate coupling regime a stepping-down procedure allows for good convergence. Even in weak coupling, if the phonon frequency is significantly lower than the hopping parameter, our adaptive method is helpful, if not necessary. By determining ground state properties as a function of decreasing phonon frequency we have established a connection between numerical results at small but non-zero phonon frequency, and adiabatic limit results obtained by using a semi-classical iterative procedure. It is clear that in one dimension no weak coupling perturbation regime exists, while in two dimensions (and higher) a definite weak coupling regime exists, and results derived within perturbation theory agree well with numerical results down to very low frequencies.
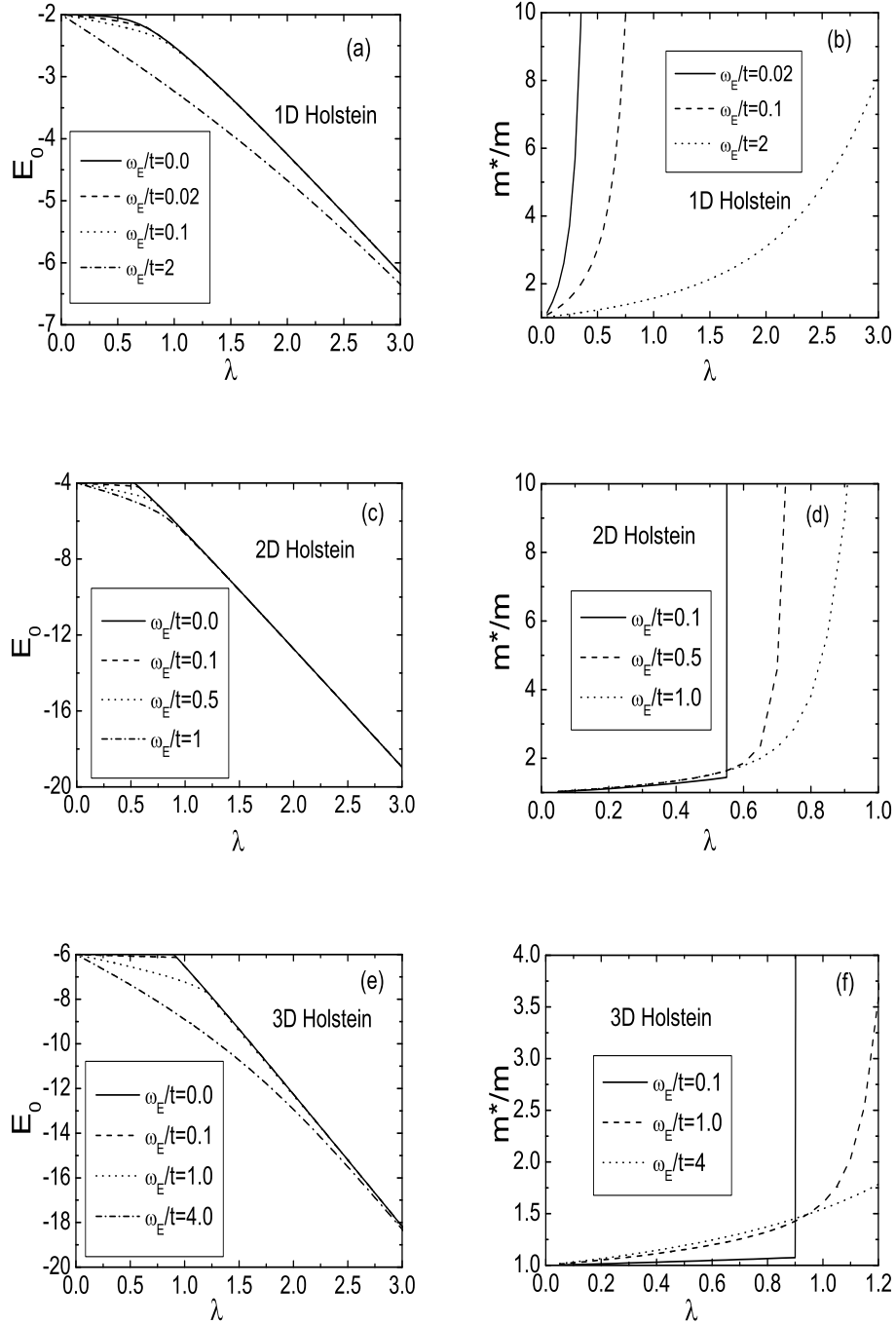
Figure 2.6: The ground state energy and effective mass vs electron phonon coupling strength for the Holstein model. The energy ((a) (c) (e)) and effective mass ((b) (d) (f)) are plotted in one, two, and three dimensions, respectively. Note the very abrupt crossover to polaron-like behaviour in 2D and 3D, both at relatively low coupling strengths. The strong coupling limit agrees very well with the adiabatic limit in all three dimensions. Also note that in (a), (c) and (e) there are three curves that are indistinguishable for $\lambda \gtrsim 1.5$, showing that the strong coupling and adiabatic regime is readily achieved for moderate λ and non-zero ω_E.

Finally, as the phonon frequency decreases, more and more phonons are present in the ground state wave function, and these lead to anomalies in the electron dispersion relation. It is somewhat ironic that the most significant polaronic effects occur in the adiabatic regime, as $\omega_E/t \to 0$. This is where weak coupling perturbation theory breaks down completely. The second order result, which is simply the so-called non-crossing approximation, fails to capture the rapid onset of multi-phonon excitations that form an integral part of the ground state wave function, as exemplified, for example, in Eq. 2.2; this is a breakdown that, for example, Alexandrov (2001) has repeatedly emphasized. At the same time, the so-called Migdal approximation, so key to the Eliashberg theory of superconductivity, is valid only in this limit. One then requires an understanding of how polaronic effects become minimized as more and more electrons are included in the problem. Apparently Pauli blocking plays an important role in mitigating the multi-phonon processes that constitute a single polaron.

CHAPTER 3

Rashba-Holstein Polaron [1]

3.1 Introduction

In much of condensed matter (magnetism excepted), the spin and orbital components of an electron are treated as independent degrees of freedom. Nonetheless, the non-relativistic approximation to the Dirac equation leads directly to the so-called Thomas term in the effective Hamiltonian, which can be written as a spin-orbit coupling term (Sakurai, 1967). This coupling can play a significant role in the electronic structure of semiconductors and metals, as documented, for example, in Winkler (2003). More recently, interest has grown because of the burgeoning possibilities in the so-called field of *spintronics*, where the spin degree of freedom is specifically exploited for potential applications (Wolf et al., 2001). Control of spin will require coupling to the orbital motion, and hence spin-orbit coupling may play a critical role in understanding and exploiting various properties of such systems.

Spin-orbit coupling, as described by Rashba (1960) is expected to be prominent in two dimensional systems that lack inversion symmetry, including surface states.

---

[1]A version of this chapter has been published. Zhou Li et.al, 2011, Phys. Rev. B 83, 195104.

Many such systems have now been identified, among which are, for example, surface alloys, Li/W(110) (Rotenberg et al., 1999), Pb/Ag(111) (Pacilé et al., 2006; Ast et al., 2007) and Bi/Ag(111) (Ast et al., 2007). In all of these systems the possibility of other interactions remains; in particular recent work (Cappelluti et al., 2007a,b; Grimaldi et al., 2006b,a) has focussed on the electron-phonon interaction, in the presence of Rashba spin-orbit interactions. In the first reference of Cappelluti et al. (2007a,b) and Grimaldi et al. (2006b,a), for example, the effective mass due to the electron-phonon interaction was shown, in weak coupling, to be enhanced by the spin-orbit interaction.

More recently, attention has focussed on the properties of a single electron interacting with oscillator degrees of freedom in the presence of Rashba spin-orbit coupling (Li et al., 2007; Chen et al., 2007; Covaci and Berciu, 2009). The first two papers investigated the behaviour of an electron (described by a parabolic band) interacting with phonons through a Fröhlich coupling. The latter paper utilized the so-called momentum average (MA) approximation (Berciu, 2006) to examine the properties of a single polaron also in the presence of spin-orbit coupling, but for a tight-binding model; in this case the electron-phonon interaction was described by the Holstein model (Holstein, 1959a,b). It is difficult to say at this point whether the Holstein model provides a particularly realistic description of real materials. However, we investigate its properties here, partly to illustrate qualitative features of the model, with the hope that they can eventually be seen in experiments, and partly because this is the model that has been utilized most in studies of polarons in general (Fehske and Trugman, 2007; Alexandrov, 2007). Moreover, and this is connected to the second reason, some of the exact methods employed here and in the references only work for the Holstein model; other models with more structure in the interaction are not so readily solvable by exact methods.

Returning to the results of Covaci and Berciu (2009), they found that the effective mass generally decreases as a function of spin-orbit coupling, V_S; however, in the weak electron-phonon coupling limit, there is initially an increase in effective mass, in agreement with Cappelluti et al (Cappelluti et al., 2007a). In this chapter we will present exact solutions to this problem, using Trugman's method (Trugman, 1990; Bonča et al., 1999), along with some modified algorithms (Li et al., 2010), so that we can span the entire parameter regime. It turns out that the MA method is fairly accurate over the entire parameter range, except for low phonon frequency.

As mentioned earlier, at this point only the Holstein model is amenable to an exact solution. For this reason we would like to make a comparison to results obtained with the MA approximation. The MA approximation can be applied to other models, and can also be investigated at higher energy scales. To aid in our understanding of the results we also develop a strong coupling expansion, based on the Lang-Firsov transformation (Lang and Firsov, 1963), following Marsiglio (1995). As in the straightforward Holstein model, strong coupling describes fairly well the small polaron regime. Finally, the adiabatic limit of the Holstein model with Rashba spin-orbit coupling has been described recently in Grimaldi (2010), following Lagendijk and Raedt (1985) and Kabanov and Mashtakov (1993) for the simple Holstein model. In the strict adiabatic limit Grimaldi finds an intermediate state (large polaron) with the lowest energy, for coupling strengths just below that required for small polaron formation, in the presence of spin-orbit coupling (see Figs. 1 and 2 in Grimaldi (2010).

We first introduce the model of study; following Covaci and Berciu (2009) it is the Holstein model with additional Rashba spin-orbit coupling, written for a tight-binding formulation. We note some of the features of the non-interacting (with respect to phonons) model. Unlike the continuum limit (Cappelluti et al., 2007a),

there is not a singularity at the bottom of the band; however, for weak spin-orbit coupling, a singularity remains very close by in energy, and causes a significant enhancement in the density of states at the bottom of the band. In Section 3.3 we present our numerical results, along with those from the strong coupling expansion and from the MA approximation. As mentioned above, the exact numerical results confirm the conclusions from Covaci and Berciu (2009). Finally, we examine the low phonon frequency and intermediate electron-phonon and spin-orbit coupling regimes, where both perturbative and MA approaches are suspect. We are unable to rule out the presence of an intermediate phase completely, but find that its occurrence is unlikely, once quantum fluctuations are included.

3.2   Model

The standard formulation for spin-orbit interaction uses two different types of electronic band structure. The first is free electron-like, which results in parabolic bands (Cappelluti et al., 2007a), and the second is tight-binding, which results in a periodic momentum dependence. While it is essentially always the case that the latter tends to the former for low electron fillings, this is not quite true when a Rashba-type spin-orbit interaction term is present. As shown in Cappelluti et al. (2007a), for example, the ground state for a single electron consists of a degenerate ring around the $\Gamma-$point. This results in an electronic density of states with a square-root singularity at the bottom of the band. For a tight-binding model, however, Covaci and Berciu (2009) pointed out that this is not the case. We will adopt a tight-binding formulation here, and examine this difference more closely in the next sub-section.

To study the single polaron with spin-orbit interaction we use a tight-binding Hamiltonian with Rashba-type spin-orbit interaction (Rashba, 1960) and a Holstein-type

(Holstein, 1959a,b) electron-phonon interaction. In real space the Hamiltonian is:

$$
\begin{aligned}
H \; = \; & -t \sum_{<i,j>,\alpha=\uparrow\downarrow} (c^\dagger_{i,\alpha} c_{j,\alpha} + c^\dagger_{j,\alpha} c_{i,\alpha}) \\
& + V_S \sum_{i,\alpha,\beta} (i c^\dagger_{i,\alpha} \sigma^{\alpha\beta}_x c_{i+\hat{y},\beta} - i c^\dagger_{i,\alpha} \sigma^{\alpha\beta}_y c_{i+\hat{x},\beta} + h.c.) \\
& - g\omega_E \sum_{i,s=\uparrow\downarrow} c^\dagger_{i,s} c_{i,s} (a_i + a^\dagger_i) + \omega_E \sum_i a^\dagger_i a_i,
\end{aligned}
\tag{3.1}
$$

where $c^\dagger_{i,s}$ $(c_{i,s})$ is the creation (annihilation) for an electron at site i with spin index s, $a^\dagger_i$ (a_i) is the creation (annihilation) operator for a phonon at site i, and $\sigma^{\alpha\beta}_x$, $\sigma^{\alpha\beta}_y$ designate the (α, β) component of the usual Pauli matrices. The sum over i is over all sites in the lattice, whereas $< i, j >$ means only nearest neighbor hopping is included. Here, as the notation already suggests, we confine ourselves to nearest neighbor hopping only. The energy scales are the hopping integral t, the strength of the Rashba spin-orbit interaction, V_S, the coupling of the electron to the oscillator degrees of freedom $g\omega_E$, and the Einstein phonon frequency, ω_E. In what follows we write all energy scales in terms of the hopping integral, t, which hereafter is set to unity. The ground-state properties of the Holstein model in one and two dimensions near the adiabatic limit have recently been studied in Li et al. (2010) and Alvermann et al. (2010). Normally spin is not considered, since this ground state is degenerate with respect to spin. As the Rashba spin-orbit interaction is turned on, however, the two-fold degeneracy will be lifted.

3.2.1 Non-interacting model: ground state and effective mass

To examine this model in detail, we use a 2×2 matrix to describe the spin sector, and begin by excluding the phonon part of the Hamiltonian. The remaining Hamiltonian

is diagonalized through Bloch states in momentum space, written as

$$H_0 = \sum_{\mathbf{k},\alpha} \epsilon_{\mathbf{k}} c^{\dagger}_{\mathbf{k},\alpha} c_{\mathbf{k},\alpha} + \sum_{\mathbf{k},\alpha,\beta} \mathbf{\Omega_k} \cdot \sigma_{\alpha\beta} c^{\dagger}_{\mathbf{k},\alpha} c_{\mathbf{k},\beta} \tag{3.2}$$

where $\epsilon_{\mathbf{k}} = -2t[\cos(k_x) + \cos(k_y)]$ and $\mathbf{\Omega_k} \cdot \sigma = 2V_S[\sin(k_y)\sigma_x - \sin(k_x)\sigma_y]$ (we set the lattice spacing a equal to unity). Diagonalizing this 2×2 matrix, we get two bands, which we name the upper and lower Rashba bands and we use the plus and minus sign to refer to these two bands, respectively. The eigenvalues and eigenstates are given by

$$H_0 \Psi_{\pm} = \varepsilon_{k,\pm} \Psi_{\pm}, \tag{3.3}$$

with eigenvalues

$$\varepsilon_{k,\pm} = -2t[\cos(k_x) + \cos(k_y)] \pm 2V_S \sqrt{\sin^2(k_y) + \sin^2(k_x)}, \tag{3.4}$$

and eigenvectors

$$\Psi_{\pm} = \frac{1}{\sqrt{2}} \left[c^{\dagger}_{k\uparrow} \pm \frac{\sin(k_y) - i\sin(k_x)}{\sqrt{\sin^2(k_y) + \sin^2(k_x)}} c^{\dagger}_{k\downarrow} \right] |0\rangle. \tag{3.5}$$

In contrast to the model with parabolic bands, this model has a four-fold degenerate ground state located at $k_x = k_y = \pm \arctan(\frac{V_S}{\sqrt{2}t})$, which can be seen clearly from a contour plot of the lower Rashba band in Fig. 3.1. There are also four saddle points near the energy minimum points, which are located at $k_x = 0, k_y = \pm \arctan(\frac{V_S}{t})$ and $k_y = 0, k_x = \pm \arctan(\frac{V_S}{t})$. As V_S increases, the separation between minimum points and saddle points is enhanced (see below, in Fig. 3.2(b)). The ground state energy for H_0 is given by $E_0 = -4t\sqrt{1 + V_S^2/(2t^2)}$. Similarly, the effective mass
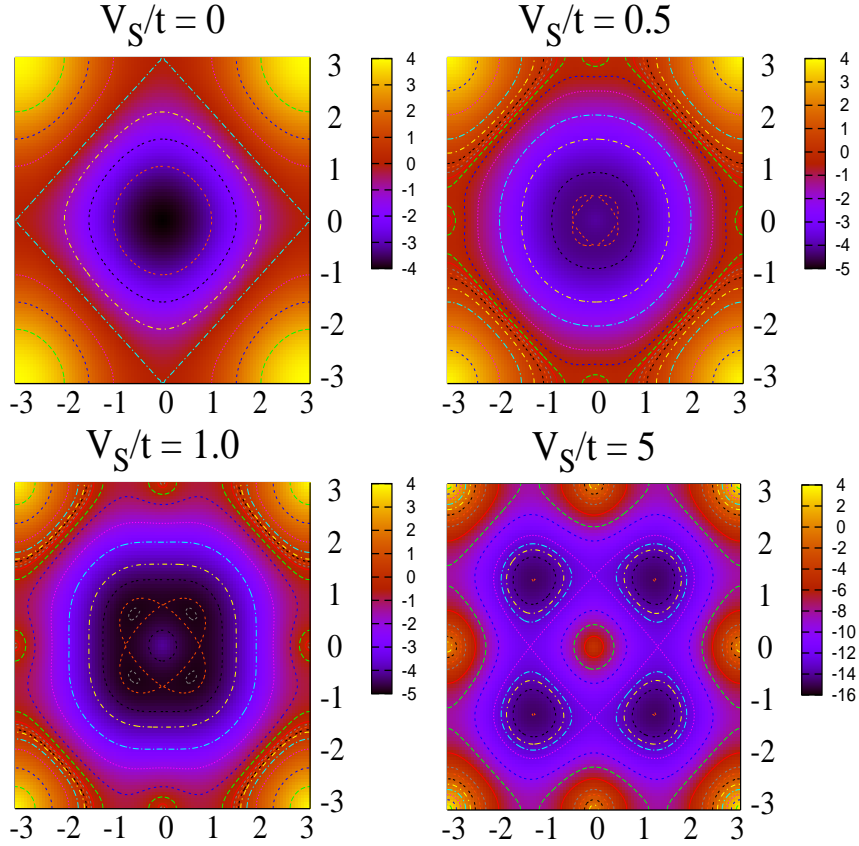
Figure 3.1: Contour plots for lower Rashba band with $V_S/t = 0, 0.5, 1.0, 5.0$. For $V_S = 0$, there is only one energy minimum point at $k_x = k_y = 0$. For $V_S > 0$, there are four energy minimum points located at $k_x = k_y = \pm \arctan(\frac{V_S}{t\sqrt{2}})$. For nonzero V_S, there are also four saddle points near the energy minimum points, which are located at $k_x = 0, k_y = \pm \arctan(\frac{V_S}{t})$ and $k_y = 0, k_x = \pm \arctan(\frac{V_S}{t})$. As V_S increases, the separation between minimum points and saddle points is increased (see Fig.3.2(b)).

along the diagonal is

$$\frac{m_{\mathrm{SO}}}{m_0} = \frac{1}{\sqrt{1 + V_S^2/(2t^2)}}, \tag{3.6}$$

where $m_0 \equiv 1/(4t)$ is the bare mass in the absence of spin-orbit interaction, and m_{SO} is the effective mass due solely to spin-orbit interaction. Note that the effective mass decreases due to spin-orbit interaction. Below we will turn on the electron phonon interaction, and the ground state energy (effective mass) will be further lowered (raised) due to polaronic processes.

3.2.2 Non-interacting model: electron density of states

The non interacting electron density of states (DOS) is defined for each band, as

$$D_s(E) = \sum_k \delta(E - \epsilon_{ks}) \tag{3.7}$$

with $s = \pm 1$.

In the main frame of Fig. 3.2(a) we show the low energy DOS for various values of the spin orbit interaction V_S; note that this involves only $D_-(E)$ as the upper Rashba band exists only at higher energies. Furthermore, information concerning the upper Rashba band can always be obtained through the symmetry

$$D_+(E) = D_-(-E). \tag{3.8}$$

Fig. 3.2(a) shows that a divergence introduced by the spin orbit interaction exists at higher energy (Covaci and Berciu, 2009) and not at the bottom of the band, as occurs for a parabolic dispersion (Cappelluti et al., 2007a). This shift is due to the separation of the energy minima from the saddle points in k-space, as shown in Fig. 3.2(b). The saddle point energy is given by $E_{\mathrm{sad}} = -2t(1 + \sqrt{1 + (V_S/t)^2})$,
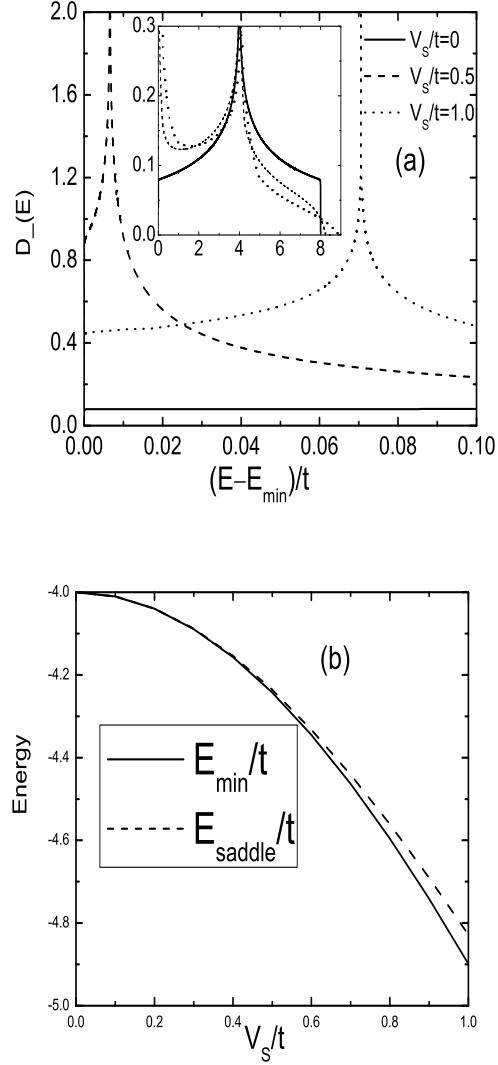
Figure 3.2: (a) Non-interacting density of states $D_-(E)$ near the bottom of the band for $V_S/t = 0, 0.5, 1.0$. In the inset the density of states in the whole band is shown for the same parameters. Note that the divergence at the bottom of the band has been shifted to higher value.(Covaci and Berciu, 2009) (b) The separation between energy minimum points and saddle points as a function of spin orbit interaction V_S/t.

which is very close to the minimum energy E_0 even for sizeable V_S/t, as is evident from the figure. This proximity of the divergence serves to elevate the value of the DOS at the bottom of the band. With no spin orbit coupling this value is $D_\pm(E = E_0 = -4t) = 1/(4\pi t)$ ($V_S = 0$). With spin orbit coupling, however, an expansion around the minimum energy $E_0 = -4t\sqrt{1 + V_S^2/2t^2}$ yields a DOS value

$$D_-(E = E_0) = \frac{\sqrt{2}}{\pi}\frac{1}{V_S} \qquad V_S \neq 0. \tag{3.9}$$

Thus a discontinuity occurs as the spin orbit coupling is changed from zero — the DOS immediately has a divergence at the bottom of the band which, for any non-zero value of V_S, shifts to slightly higher energy. The inset shows $D_-(E)$ over a wider energy range. Further details are provided in Appendix B.

3.3   Ground state energy and effective mass

When the electron phonon interaction is turned on, the ground state energy (effective mass) will be lowered (increased) due to polaron effects. To study the polaron problem numerically, we adopt the variational method outlined by Trugman and coworkers (Trugman, 1990; Bonča et al., 1999), which could determine polaron properties in the thermodynamic limit accurately. This method was described in detail in Chapter 1 and 2.

3.3.1   Strong coupling theory

To investigate the strong coupling regime of the Rashba-Holstein model for a single polaron, we use the Lang-Firsov (Lang and Firsov, 1963; Marsiglio, 1995) unitary

transformation $\overline{H} = e^S H e^{-S}$, where $S = g \sum_{i,\sigma} n_{i,\sigma}(a_i - a_i^\dagger)$, and obtain

$$\overline{H} = \overline{H}_0 + \overline{T} \tag{3.10}$$

with

$$\overline{H}_0 = \omega_E \sum_i a_i^\dagger a_i - g^2 \omega_E \sum_{i,\sigma} c_{i,\sigma}^\dagger c_{i,\sigma} \tag{3.11}$$

and

$$
\begin{aligned}
\overline{T} = \quad &-t \sum_{i,\sigma} (c_{i,\sigma}^\dagger c_{i+\hat{x},\sigma} X_i^\dagger X_{i+\hat{x}} + c_{i,\sigma}^\dagger c_{i+\hat{y},\sigma} X_i^\dagger X_{i+\hat{y}} + h.c.) \\
&+iV_S \sum_i (c_{i,\alpha}^\dagger \sigma_x^{\alpha\beta} c_{i+\hat{y},\beta} X_i^\dagger X_{i+\hat{y}} \\
&-c_{i,\alpha}^\dagger \sigma_y^{\alpha\beta} c_{i+\hat{x},\beta} X_i^\dagger X_{i+\hat{x}} - h.c.),
\end{aligned} \tag{3.12}
$$

where $X_i^\dagger = \exp\{g(a_i - a_i^\dagger)\}$. Note that if $[A, B]$ is a c-number, we can use the identity $e^{A+B} = e^A e^B e^{-1/2[A,B]}$; then the hopping part of the Hamiltonian becomes

$$
\begin{aligned}
\overline{T} = \quad &-t e^{-g^2} \sum_{i,\sigma,\delta} [c_{i,\sigma}^\dagger c_{i+\delta,\sigma} (P_i^-)^\dagger (P_{i+\delta}^+)^\dagger P_i^+ P_{i+\delta}^- + h.c.] \\
&+iV_S e^{-g^2} \sum_i [c_{i,\alpha}^\dagger \sigma_x^{\alpha\beta} c_{i+\hat{y},\beta} (P_i^-)^\dagger (P_{i+\hat{y}}^+)^\dagger P_i^+ P_{i+\hat{y}}^- \\
&-c_{i,\alpha}^\dagger \sigma_y^{\alpha\beta} c_{i+\hat{x},\beta} (P_i^-)^\dagger (P_{i+\hat{x}}^+)^\dagger P_i^+ P_{i+\hat{x}}^- - h.c.],
\end{aligned} \tag{3.13}
$$

where $P_i^\pm \equiv \exp(\pm g a_i)$. The unperturbed bare Hamiltonian, $\overline{H}_0$ provides the zeroth order energy for the polaron, and is already diagonal for the single electron sector. The eigenvalues are given by $E_n = n\omega_E - g^2\omega_E$, where n is the total number of phonons. Clearly the ground state has $n = 0$, but remains 2N-fold degenerate, since the electron can occupy any one of the N sites and it can have either spin up or spin down. If we consider the hopping term $\overline{T}$ as a perturbation and apply degenerate

perturbation theory to the 2N-fold degenerate ground state, we need to diagonalize a $2N \times 2N$ matrix. A simpler approach is to recognize that the momentum k is a good quantum number, and if we transform the original problem into k-space, we need only solve a 2×2 matrix which mixes the spin sectors; this results in essentially Eq. (3.2), but with an extra band narrowing factor e^{-g^2}. Thus we obtain the first order perturbation correction to the energy as

$$E_{k\pm} = e^{-g^2} \varepsilon_{k\pm} - g^2 \omega_E, \tag{3.14}$$

and the result is the familiar band narrowing factor that occurs when $V_S = 0$.

The eigenstates from degenerate perturbation theory are now simply Bloch-like states, $\Psi_\pm$, as found in the non-interacting theory, Eq. (3.5). Thus the degeneracy is broken, and a comparatively narrower band is formed with a minimum at a non-zero wave vector in the lower Rashba band, as found in the non-interacting case. To find the second order correction to the ground state energy, we proceed as in Marsiglio (1995), and find

$$E_{k-}^{(2)} = \sum_{n_{TOT} \neq 0, n_1, n_2, \ldots = 0, 1, \ldots \infty} \sum_{\substack{\ell=1 \\ \sigma}}^{N}$$
$$\frac{\left| \langle n_1, n_2, \ldots n_N |_{ph} \otimes \langle c_{\ell\sigma} |_{el} \overline{T} | \Psi_{k,-} \rangle_{el} \otimes |0\rangle_{ph} \right|^2}{-n_{TOT} \omega_E} \tag{3.15}$$

where n_{TOT} is the total number of phonons and $\Psi_{k,-}$ is given in Eq. (3.5). With details shown in the appendix, we obtain

$$E_{k-}^{(2)} = -4e^{-2g^2} \frac{t^2 + V_S^2}{\omega_E} \left[f(2g^2) - f(g^2) \right] - e^{-2g^2} f(g^2) \frac{\epsilon_{k-}^2}{\omega_E}, \tag{3.16}$$

where $f(x) \equiv \sum_{n=1}^{\infty} \frac{1}{n} \frac{x^n}{n!} \approx e^x/x \left[1 + 1/x + 2/x^2 + \ldots \right]$ (see Appendix). In some of

the ensuing discussion, we will use the constant λ, familiar as the effective mass enhancement from weak coupling perturbation theory for the interacting electron gas. Here we use the definition (Li et al., 2010) $\lambda \equiv 2g^2\omega_E \frac{1}{4\pi t}$, since $1/(4\pi t)$ is the value of the non-interacting electron density of states for $V_S = 0$ at the bottom of the band. Note that our definition of λ differs from that in Covaci and Berciu (2009) or Marsiglio (1995); both use the more conventional average density of states, $1/(8t)$. Thus the ground state energy, excluding exponentially suppressed corrections, is

$$E_{GS} = -2\pi t\lambda\big(1 + 2\frac{t^2 + V_S^2}{(2\pi t\lambda)^2}\big), \tag{3.17}$$

and there is a correction of order $1/\lambda^2$ compared to the zeroth order result. Corrections in the dispersion enter in strong coupling only with an exponential suppression.

3.3.2 Weak coupling theory

In the weak electron-phonon coupling regime, does spin-orbit coupling suppress or enhance the "polaron effect" due to the electron-ion coupling? Weak coupling calculations with a parabolic electron dispersion (Cappelluti et al., 2007a) showed an *increase* in the effective mass, for example, as the spin-orbit coupling was increased. Here we perform weak coupling perturbation theory, as described in Cappelluti et al. (2007a), with the same definitions, except that the tight binding dispersion is used to describe the non-interacting electrons, as outlined in the previous section. A straightforward calculation yields the self energy to first order in λ as

$$\Sigma_{\text{weak}}(\omega + i\delta) = \pi\lambda t\omega_E \sum_{\mathbf{k},s=\pm} \frac{1}{\omega + i\delta - \omega_E - \varepsilon_{k,s}}. \tag{3.18}$$

The effective mass can be obtained by the derivative of the self energy

$$\frac{m^*_{\text{weak}}}{m_{SO}} = 1 - \frac{\partial}{\partial\omega}\Sigma_{\text{weak}}(\omega + i\delta)|_{\omega=E_0}. \tag{3.19}$$

Near the adiabatic limit ($\omega_E \to 0$), by expanding $\varepsilon_{k,-}$ around E_0, as shown in the appendix for the calculation of the DOS, we obtain

$$\frac{m^*_{\text{weak}}}{m_{SO}} = 1 + \frac{\sqrt{2}\lambda t}{V_S}, \tag{3.20}$$

which shows a diverging effective mass as the spin-orbit coupling decreases. In fact, there is a discontinuity for $V_S = 0$, as the result is simply $\frac{m^*_{\text{weak}}}{m_{SO}} = 1 + \lambda/2$, and $m_{SO} \to m_0 = 1/2t$, as given by Eq. (3.6). Eq. (3.20) will have a limited domain of validity, however, as we will see below.

3.3.3 Numerical Results

In Fig. 3.3, we show the ground state energy and the effective mass correction as a function of electron-phonon coupling λ, with non-zero values of the spin orbit interaction, $V_S/t = 0.5$ and $V_S/t = 1.0$; these are compared with the results from the Holstein model with $V_S/t = 0$. Here the phonon frequency is set to be $\omega_E/t = 1.0$, which is the typical value used in Covaci and Berciu (2009), and for each value of V_S, the ground state energy is compared to the corresponding result for $\lambda = 0$. The numerical results are compared with results from weak coupling perturbation theory and from Lang-Firsov strong coupling theory.

In Fig. 3.3(a), the ground state energy crosses over smoothly (at around $\lambda \approx 0.8$) from the delocalized electron regime to the small polaron regime. Note that there is a slight dependence of the ground state energy on the spin orbit interaction. If
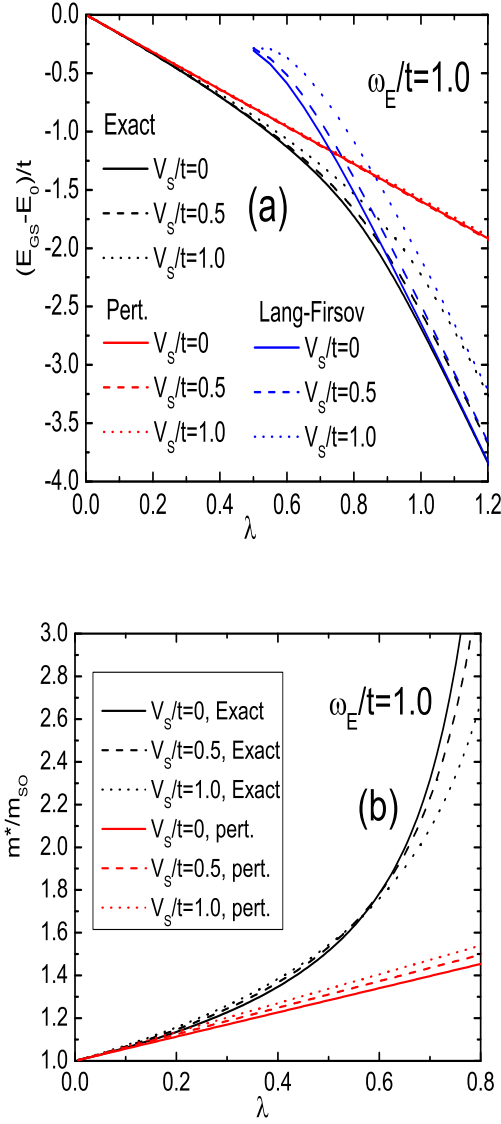
Figure 3.3: (a) Ground state energy difference $E_{GS} - E_0$ vs. λ for $V_S/t = 0, 0.5, 1.0$ and $\omega_E/t = 1.0$. Exact numerical results are compared with those from weak coupling perturbation theory (labeled "Pert." in the figure) and from Lang-Firsov strong coupling theory. Agreement of both perturbative approaches with the exact numerical result is excellent. The MA result (not shown) is also in excellent agreement with the numerical results. (b)Effective mass m^*/m_{SO} vs. λ. Numerical results are compared with that from weak coupling perturbation theory, and agreement is excellent for low values of λ. Both exact and perturbative approaches show an enhanced effective mass with increasing spin orbit coupling.
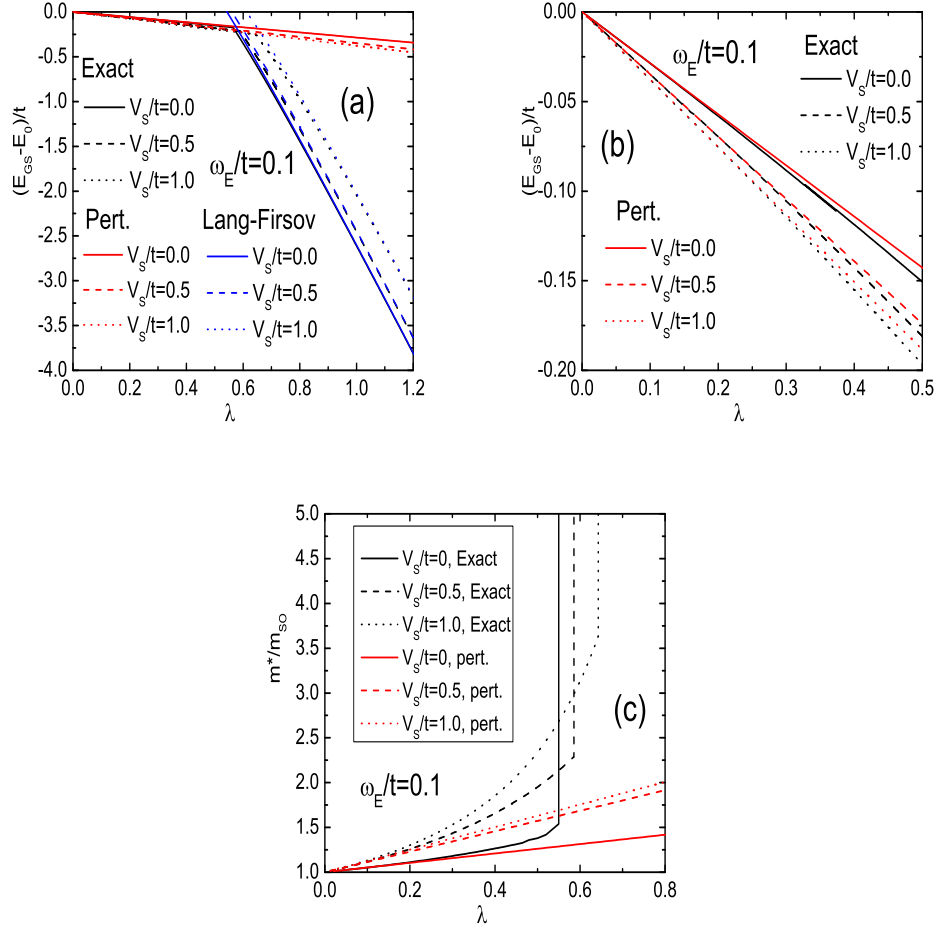
Figure 3.4: (a) Ground state energy $E_{GS} - E_0$ vs. λ for $V_S/t = 0, 0.5, 1.0$ and $\omega_E/t = 0.1$. Exact numerical results are compared with those from weak coupling perturbation theory (labeled Pert. in the fig) and Lang-Firsov strong coupling theory. (b) Ground state energy $E_{GS} - E_0$ vs. λ in the weak and intermediate coupling regime. (c) Effective mass m^*/m_{SO} vs. λ. Numerical results are compared with those from weak coupling perturbation theory.
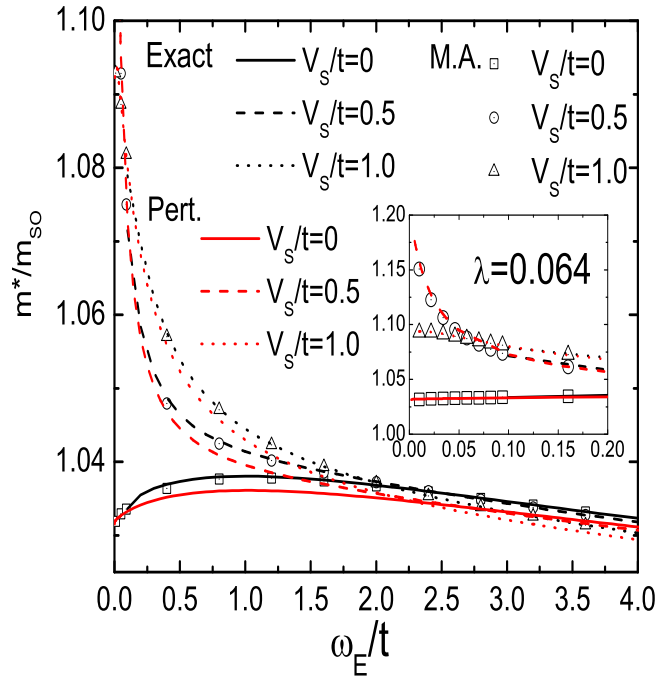
Figure 3.5:   Effective mass m^*/m_{SO} vs. ω_E/t for weak electron phonon coupling $\lambda = 0.064$. In the inset the effective mass in the phonon frequency region near the adiabatic limit is shown. It is clear that the effective mass is enhanced as spin orbit interaction decreases near the adiabatic limit. This is in agreement with the result inferred from the electron density of states shown in Fig.3.2(a).

we define $\Delta E = E_{GS} - E_0$, then $\Delta E(V_S/t = 0.5) < \Delta E(V_S/t = 0) < \Delta E(V_S/t = 1.0)$ in the delocalized electron regime, which is in agreement with the weak coupling perturbation theory, though this is barely visible in the figure. In the small polaron regime, the ground state energy is shifted up by the spin orbit interaction. This trend agrees with the results from Lang-Firsov strong coupling theory. For $V_S/t = 0$, the Lang-Firsov theory agrees very well with the numerical results, while as the spin orbit coupling V_S increases, the Lang-Firsov theory becomes less accurate for the same electron phonon coupling (e.g. if we look at $\lambda = 1.0$, for $V_S/t = 1.0$, the difference between Lang-Firsov theory and exact numerical results is larger than that for $V_S/t = 0$). This is due to the fact that the bandwidth is increased by spin orbit interaction, so the effective electron phonon coupling is decreased by spin orbit interaction. Better agreement with Lang-Firsov theory is achieved for larger values of λ. In Fig. 3.3(b), the effective mass is enhanced by the spin orbit interaction in the delocalized electron regime, which is in agreement with the prediction from weak coupling perturbation theory. Here we have only shown results in the region $V_S/t = 0 \sim 1.0$; for larger values of V_S/t the effective mass will be decreased by the spin orbit interaction in the delocalized regime. In the small polaron regime, the effective mass will always be decreased by the spin orbit interaction.

In Fig. 3.4, we show the same results as Fig. 3.3 for a much smaller phonon frequency $\omega_E/t = 0.1$, which is closer to the adiabatic limit. In Fig. 3.4(a), the ground state energy crosses over sharply (but still smoothly) from the delocalized electron regime to the small polaron regime. If we use λ_c to describe the critical value for this sharp crossover, λ_c will be enhanced significantly by the spin orbit interaction. For $V_S/t = 0.0, \lambda_c \simeq 0.55$, while for $V_S/t = 5.0$, $\lambda_c \simeq 1.55$ from our numerical results. In Fig. 3.4(b), in the delocalized electron regime the ground state energy is decreased by the spin orbit interaction $\Delta E(V_S/t = 1.0) < \Delta E(V_S/t = 0.5) < \Delta E(V_S/t = 0.0)$,

which is also in agreement with the weak coupling perturbation theory. For larger V_S/t the ground state energy will be increased in the delocalized electron regime. In the small polaron regime, the ground state energy will be increased by the spin orbit interaction, in agreement with the Lang-Firsov theory. In Fig. 3.4(c), the effective mass enhancement for different spin orbit interaction V_S/t is shown vs. electron phonon coupling strength, λ. For $V_S/t = 0$ there is a rather sharp crossover from the delocalized electron regime to the small polaron regime (Li et al., 2010).

Near the crossover point, the effective mass enhancement for the delocalized electron is around 1.4. For nonzero $V_S/t < 1$, near the crossover point, the effective mass enhancement is higher, but still within the same order of magnitude as $V_S/t = 0$. Grimaldi (Grimaldi, 2010) recently studied the Holstein model with spin-orbit coupling in the strict adiabatic limit ($\omega_E = 0$). He found that for nonzero spin orbit interaction V_S, the ground state will experience two phase transitions as the electron phonon coupling λ is increased. The first transition is from a delocalized electron to a large polaron, while the second one is from a large polaron to a small polaron. As is well known, inclusion of quantum effects in the phonons (non-zero ω_E) replaces the transitions with crossovers. As seen in Fig. 3.4(c), only the crossover from a delocalized electron to a small polaron remains sharp; the distinction between a delocalized electron and a large polaron is not apparent in our calculations. Our results did not exclude the possibilities that a more well-defined large polaron regime will be found for $\omega_E/t < 0.1$, although we find this possibility unlikely. A similar circumstance holds in the absence of a spin orbit coupling, where the adiabatic approximation gives rise to a single transition, while the quantum calculations results only in a crossover. Smaller values of ω_E can be explored, but quantum fluctuations become stronger for $\omega_E/t < 0.1$ and the problem is numerically expensive for intermediate electron phonon coupling.
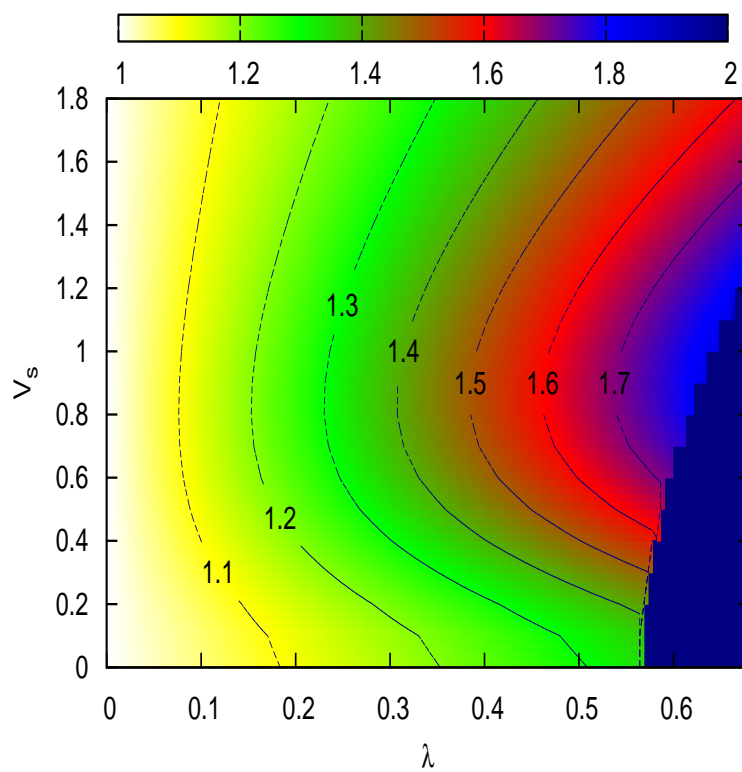
Figure 3.6:   Effective mass m^*/m_{SO} map as a function of spin orbit interaction V_S/t and coupling constant λ for $\omega_E/t = 0.1$ obtained with the momentum average approximation. Credit from Lucian Covaci.
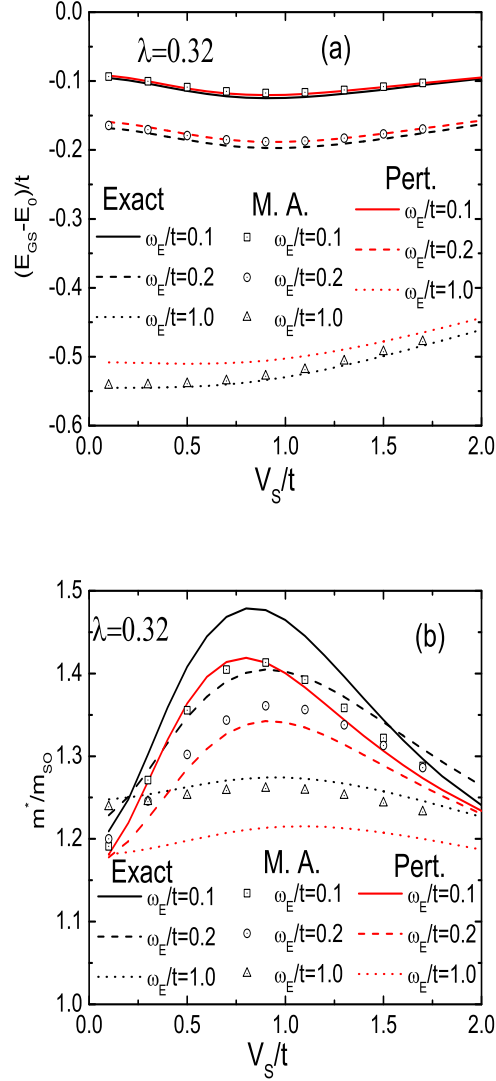
Figure 3.7: (a) Ground state energy $E_{GS} - E_0$ as a function of spin orbit interaction V_S/t for $\omega_E/t = 0.1, 0.2, 1.0$ at $\lambda = 0.32$. (b) Effective mass m^*/m_{SO} as a function of spin orbit interaction V_S/t for the same parameters. Exact numerical results are compared with those from momentum averaging methods and weak coupling perturbation theory. The Momentum Average approximation does not do as well for low phonon frequencies.

To obtain some insight for the polaron effective mass near the adiabatic limit, we resort to weak coupling perturbation theory. In Fig. 3.5 we observe an anomalous increase of the effective mass for small ω_E for nonzero V_S. However, the effective mass stops increasing as it reaches some finite number (around 1.2 and 1.1 for $V_S/t = 0.5$ and 1.0, respectively), so this does not indicate a breakdown of the perturbation theory. This result is confirmed by the M.A. results obtained from Lucian Covaci, as illustrated. This is also in agreement with results from the adiabatic limit. As shown in Fig. 2 of Grimaldi (2010), for $V_S/t = 0.5$ and 1.0 (his $\gamma/t = 1.0$ and 2.0), the electron is definitely in the delocalized electron regime for $\lambda = 0.064$ ($\lambda = 0.1$ in (Grimaldi, 2010). Actually this anomalous increase of effective mass is caused by an increase in the value of the electron DOS at the bottom of the band, as shown in Fig.3.2 and Eq. (3.9). Thus, for even smaller values of V_S/t, the anomalous mass enhancement will increase further and perturbation theory will eventually break down. This is in agreement with the adiabatic limit results — as Fig. 2 of Grimaldi (2010) shows, for $V_S/t \simeq 0$, the electron enters the large polaron regime for small λ. As mentioned earlier, our results are consistent with crossovers rather than transitions. This can be also seen in Fig. 3.6 where we plot for completeness a map of the effective mass as a function of V_s/t and λ obtained by using the MA approximation for $\omega_E/t = 0.1$. The exact results, while different in the details, show the same qualitative trends.

In Fig. 3.7, we compare exact numerical results with both the momentum average method (Covaci and Berciu, 2009) and with weak coupling perturbation theory, for different values of ω_E. In Fig. 3.7(a), the ground state energy is shown as a function of V_S/t, while in Fig. 3.7(b), the effective mass is shown as a function of V_S/t. The MA method agrees well with the exact numerical results for $\omega_E/t = 1.0$. For smaller values of ω_E ($\omega_E/t = 0.1$ and 0.2), the Momentum Average approximation becomes

less accurate and agrees more closely with weak coupling perturbation theory. This is similar to what happens for the Holstein model. Reasons for this quantitative failure of MA in the adiabatic limit are explained in Berciu (2006).

3.4   Chapter Summary

In this chapter we have studied the problem of a single electron coupled to oscillating ions, in the presence of a spin-orbit interaction. This problem may be important for a variety of spintronics applications, as even an alteration of the effective mass can impact the coupling of spin and charge degrees of freedom. Many previous treatments have addressed this problem with a finite density of electrons, and have therefore necessarily required approximate theoretical methods for solution. The limit of only one electron, previously solved with weak coupling perturbation methods and with the momentum average approximation, is amenable to exact solution as described here, and serves as a benchmark to which other, approximate solutions must converge. Moreover, in many dilute semiconductor applications, the single electron result may be the relevant regime required for understanding of the problem.

The exact method of solution utilizes the Trugman method of solution, (Bonča et al., 1999) through Lanczos diagonalization. The procedure for this is now well documented, and converges very quickly over a very wide parameter regime. The momentum average approximation (Covaci and Berciu, 2009) also works very well over the entire parameter regime; there is a breakdown for very low phonon frequencies. In this regime the adiabatic approximation (Grimaldi, 2010) provides a good qualitative picture. Weak coupling perturbation theory (Cappelluti et al., 2007a) tends to be fairly accurate only for very small coupling strengths. Finally, strong

coupling perturbation theory (Marsiglio, 1995) is very accurate in the small polaron regime.

In weak coupling the presence of spin orbit coupling increases the effective mass of the electron coupled to Einstein phonons (Cappelluti et al., 2007a). The effective mass is small to begin with, so in this regime the impact of spin orbit coupling is fairly minor. As the electron phonon coupling increases, and one enters the small polaron regime, the presence of spin orbit coupling has the opposite effect, as first noted with the momentum average approximation (Covaci and Berciu, 2009). Since in this regime the effective masses can be quite large, spin orbit coupling can have a profound effect on the characteristics of the electron.

CHAPTER 4

Dresselhaus-Rashba-Holstein Polaron [1]

4.1   Introduction

One of the end goals in condensed matter physics is to achieve a sufficient under-standing of materials fabrication and design so as to 'tailor-engineer' specific desired properties into a material. Arguably *pn*-junctions long ago represented some of the first steps in this direction; nowadays, heterostructures (Bimberg et al., 1999) and mesoscopic geometries (Y.Murayama, 2001) represent further progress towards this goal.

In the field of *spintronics*, where the spin degree of freedom is specifically exploited for potential applications (Wolf et al., 2001; Koralek et al., 2009), spin-orbit coupling (Winkler, 2003) plays a critical role because control of spin will require coupling to the orbital motion. Spin orbit coupling, as described by Rashba (Rashba, 1960) and Dresselhaus (Dresselhaus, 1955), is expected to be prominent in two dimensional systems that lack inversion symmetry, including surface states. These different

---

[1]Accepted by Phys. Rev. B.

kinds of coupling are in principle independently controlled (Maiti et al., 2011; Meier et al., 2007).

The coexistence of Rashba and Dresselhaus spin-orbit coupling has now been realized in both semiconductor quantum wells (Meier et al., 2007; Koralek et al., 2009) and more recently in neutral atomic Bose-Einstein condensate (Lin et al., 2011). When the Rashba and (linear) Dresselhaus spin-orbit coupling strengths are tuned to be equal, SU(2) symmetry is predicted to be recovered and the persistent spin helix state will emerge (Bernevig et al., 2006; Koralek et al., 2009; Lin et al., 2011). This symmetry is expected to be robust against spin-independent scattering but is broken by the cubic Dresselhaus spin-orbit coupling and other spin-dependent scattering which may be tuned to be negligible (Koralek et al., 2009).

While we focus on the spin-orbit interaction, other interactions are present. In particular, the electron-phonon interaction will be present and may be strong in semiconductor heterostructures. Moreover, optical lattices (Bloch et al., 2008) with cold polar molecules may be able to realize a tuneable Holstein model (Herrera and Krems, 2011). The primary purpose of this work is to investigate the impact of electron-phonon coupling (as modeled by the Holstein model (Holstein, 1959a,b)) on the properties of the spin-orbit coupled system. We will utilize a tight-binding framework; previously it was noted that in the presence of Rashba spin-orbit coupling the vicinity of a van Hove singularity near the bottom of the electron band (Cappelluti et al., 2007a,b; Covaci and Berciu, 2009; Li et al., 2011) had a significant impact on the polaronic properties of an electron; with additional (linear) Dresselhaus spin-orbit coupling the van Hove singularity shifts well away from the band bottom, as the two spin-orbit couplings acquire equal strength. As we will illustrate below, the presence of two separately tunable spin-orbit couplings will result in significant controllability of the electron effective mass.

4.2 Model and methodologies

We use a tight-binding model with dimensionless Holstein electron-phonon coupling of strength g, and with linear Rashba (V_R) and Dresselhaus (V_D) spin-orbit coupling:

$$
\begin{aligned}
H &= -t \sum_{<i,j>,s=\uparrow\downarrow} (c_{i,s}^\dagger c_{j,s} + c_{j,s}^\dagger c_{i,s}) \\
&\quad +i \sum_{j,\alpha,\beta} (c_{j,\alpha}^\dagger \hat{V}_1 c_{j+\hat{y},\beta} - c_{j,\alpha}^\dagger \hat{V}_2 c_{j+\hat{x},\beta} - h.c.) \\
&\quad -g\omega_E \sum_{i,s=\uparrow\downarrow} c_{i,s}^\dagger c_{i,s}(a_i + a_i^\dagger) + \omega_E \sum_i a_i^\dagger a_i
\end{aligned}
\tag{4.1}
$$

where $c_{i,s}^\dagger (c_{i,s})$ creates (annihilates) an electron at site i with spin index s, $a_i^\dagger (a_i)$ creates (annihilates) a phonon at site i. The operators $\hat{V}_j$, $j = 1, 2$ are written in terms of the spin-orbit coupling strengths and the Pauli matrices as $\hat{V}_1 = V_R\hat{\sigma}_x - V_D\hat{\sigma}_y$, and $V_2 = V_R\hat{\sigma}_y - V_D\hat{\sigma}_x$, The sum over i is over all sites in the lattice, whereas $< i, j >$ signifies that only nearest neighbour hoppings is included. Other parameters in the problem are the phonon frequency, ω_E, and the hopping parameter t, which hereafter is set equal to unity.

Without the electron-phonon interaction the electronic structure is readily obtained by diagonalizing the Hamiltonian in momentum space. With the definitions

$$
\begin{aligned}
S_1 &\equiv V_R\sin(k_y) + V_D\sin(k_x), \\
S_2 &\equiv V_R\sin(k_x) + V_D\sin(k_y),
\end{aligned}
\tag{4.2}
$$
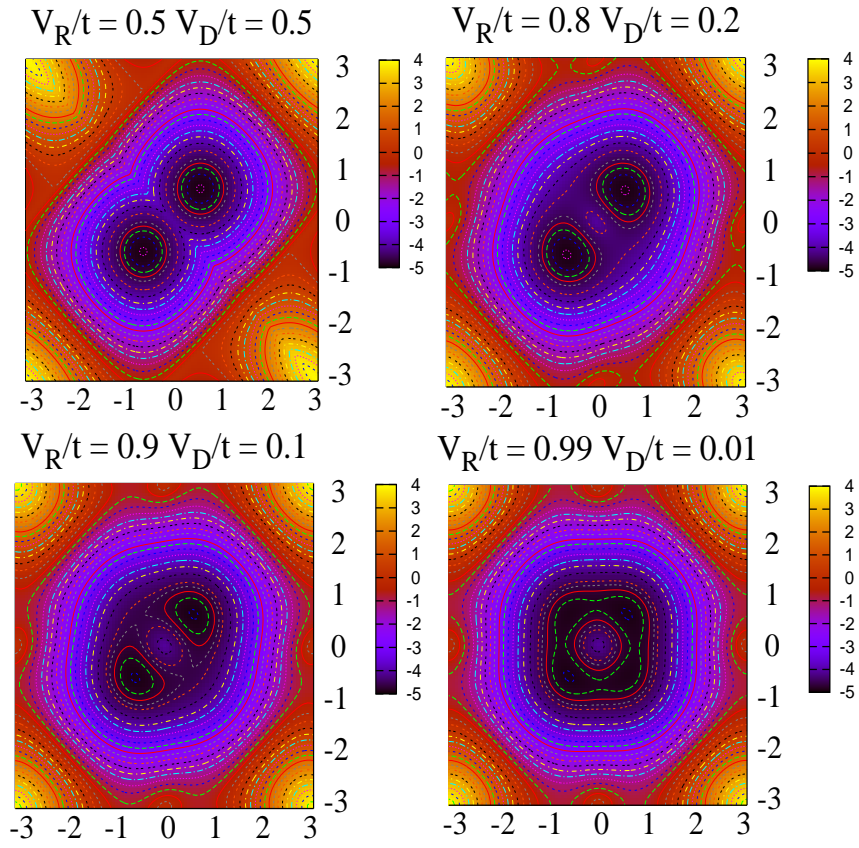
Figure 4.1: Contour plots for the bare energy bands with Rashba-Dresselhaus spin-orbit coupling, for different values of V_R and V_D while the sum is kept constant: $V_R + V_D = t$ for these cases. (a) $V_R = V_D = 0.5t$, (b) $V_R = 0.8t, V_D = 0.2t$, (c) $V_R = 0.9t, V_D = 0.1t$, and (d) $V_R = 0.99t, V_D = 0.01t$. Note the clear progression from a two-fold degenerate ground state to a four-fold degenerate one.

we obtain the eigenvalues

$$\varepsilon_{k,\pm} = -2t[\cos(k_x) + \cos(k_y)] \pm 2\sqrt{S_1^2 + S_2^2} \tag{4.3}$$

and eigenvectors

$$\Psi_{k\pm} = \frac{1}{\sqrt{2}} \left[c_{k\uparrow}^\dagger \pm \frac{S_1 - iS_2}{\sqrt{S_1^2 + S_2^2}} c_{k\downarrow}^\dagger \right] |0\rangle. \tag{4.4}$$

The ground state energy is

$$E_0 = -4t\sqrt{1 + (V_R + V_D)^2/(2t^2)}. \tag{4.5}$$

Without loss of generality we can consider only $V_R \geq 0$ and $V_D \geq 0$. Either Rashba and Dresselhaus spin-orbit coupling independently behave in the same manner, and give rise to a four-fold degenerate ground state with wave vectors, $(k_x, k_y) = (\pm \arctan(\frac{V_R}{\sqrt{2}t}), \pm \arctan(\frac{V_R}{\sqrt{2}t}))$, $(V_D = 0)$, and similarly for $V_D \neq 0$ and $V_R = 0$. With both couplings non-zero, however, the degeneracy becomes two-fold, with the ground state wave vectors,

$$(k_{x0}, k_{y0}) = \pm(k_0, k_0); \quad \text{where} \quad k_0 = \tan^{-1}(\frac{V_R + V_D}{\sqrt{2}t}). \tag{4.6}$$

It is clear that the sum of the coupling strengths replaces the strength of either in these expressions,(Li et al., 2011) so that henceforth in most plots we will vary one of the spin-orbit interaction strengths while maintaining their sum to be fixed. Similarly, the effective mass, taken along the diagonal, is

$$\frac{m_{\text{SO}}}{m_0} = \frac{1}{\sqrt{1 + (V_R + V_D)^2/(2t^2)}}, \tag{4.7}$$

where $m_0 \equiv 1/(2t)$ (lattice spacing, $a \equiv 1$, and $\hbar \equiv 1$) is the bare mass in the

absence of spin-orbit interaction, and m_{SO} is the effective mass due solely to the spin-orbit interaction.

The non interacting electron density of states (DOS) is defined for each band, as

$$D_s(\epsilon) = \sum_k \delta(\epsilon - \epsilon_{ks}) \tag{4.8}$$

with $s = \pm 1$.

In Fig. 4.2(a) we show the low energy DOS for various values of the spin-orbit coupling strengths, V_R and V_D, while keeping their sum constant; the low energy van Hove singularity disappears for $V_R = V_D$. Note that only $D_-(\epsilon)$ is shown as the upper band, with DOS $D_+(\epsilon)$, exists only at higher energies. Furthermore, information concerning the upper band can always be obtained through the symmetry

$$D_+(\epsilon) = D_-(-\epsilon). \tag{4.9}$$

In Fig. 4.2(b) we show the value of the density of states at the bottom of the band vs. V_D; The DOS value at the minimum energy is given by

$$D_-(E_0) = \frac{1}{2\pi t} \frac{1}{\sqrt{1 + \frac{(V_R+V_D)^2}{2t^2} - \frac{(V_R-V_D)^2}{(V_R+V_D)^2}}} \tag{4.10}$$

Note that when the coupling strengths are equal, the density of states has a minimum. Also note that when one kind of spin-orbit coupling vanishes, e.g. $V_R = 0$, or $V_D = 0$, there will be a discontinuity for the density of states (the density of states jumps to twice its value). This is caused by a transition from a doubly degenerate ground state to a four-fold degenerate ground state. This discontinuity will also appear for $V_D \simeq 0$ or $V_R \simeq 0$ near the bottom of the band as can be seen from Fig. 4.2(a) for $V_R = 0.99, V_D = 0.01$.
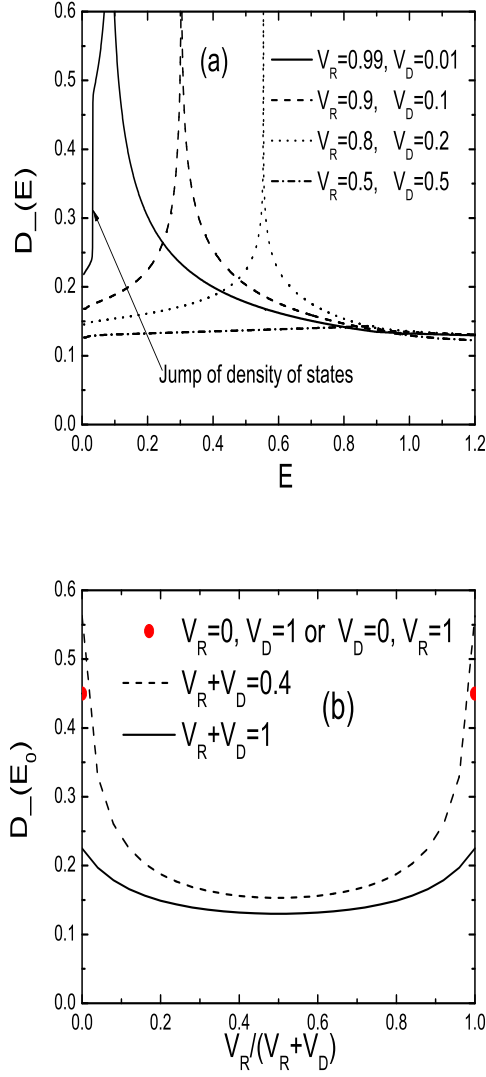
Figure 4.2: (a)The non-interacting density of states $D_{(}E)$ near the bottom of the band for four values of the spin-orbit coupling strengths: $(V_R, V_D)/t = (0.5, 0.5)$ (dot-dashed curve), $(0.8, 0.2)$ (dotted curve), $(0.9, 0.1)$ (dashed curve), and $(0.99, 0.01)$ (solid curve). Note that for equal coupling strengths there is no van Hove singularity at low energies. (b) The value of the density of states at the bottom of the band (ground state) as a function of V_D (while the total coupling strength, $V_R + V_D$, is held constant. The value of the density of states is at a minimum when $V_R = V_D$. For $V_R = 0$ or $V_D = 0$ there is a discontinuity, caused by the transition from a doubly degenerate ground state to a four-fold degenerate ground state.

4.3 Electron-phonon interaction.

As the electron phonon interaction is turned on, the ground state energy (effective mass) will decrease (increase) due to polaron effects. To study the polaron problem numerically, we adopt the variational method outlined by Trugman and coworkers (Trugman, 1990; Bonča et al., 1999), which is a controlled numerical technique to determine polaron properties in the thermodynamic limit exactly. This method was recently further developed (Li et al., 2010; Alvermann et al., 2010) to study the polaron problem near the adiabatic limit with Rashba spin-orbit coupling (Li et al., 2011). This case was also studied in Covaci and Berciu (2009) using the Momentum Average Approximation (Berciu, 2006).

In Fig. 4.3, we show the ground state energy and the effective mass correction as a function of the electron phonon coupling $\lambda \equiv 2g^2\omega_E/(4\pi t)$,(Li et al., 2010) for various spin-orbit coupling strengths, but with the sum fixed: $V_R + V_D = t$. These are compared with the results from the Rashba-Holstein model with $V_D = 0$. Here the phonon frequency is set to be $\omega_E/t = 1.0$, which is the typical value used in Covaci and Berciu (2009), and for each value of V_R, the ground state energy is compared to the corresponding result for $\lambda = 0$. The numerical results are compared with results from the MA method obtained from Lucian Covaci and from Lang-Firsov strong coupling theory (Lang and Firsov, 1963; Marsiglio, 1995). In Fig. 4.3(a), the ground state energy crosses over smoothly (at around $\lambda \approx 0.8$) from the delocalized electron regime to the small polaron regime. In the whole regime, the ground state energy is shifted up slightly as the Dresselhaus spin-orbit coupling, V_D, is increased in lieu of the Rashba spin-orbit coupling. We show results for $V_D \leq V_R$, as the complementary regime is completely symmetric. The MA results agree very well with the exact results and the Lang-Firsov strong coupling results agree well in the
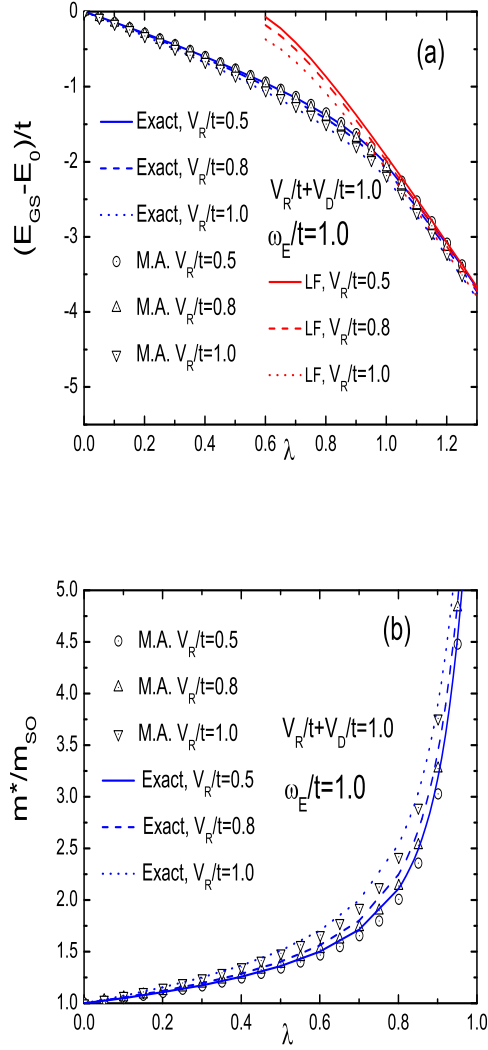
Figure 4.3: (a) Ground state energy difference $E_{GS} - E_0$ vs. λ for $V_R/t = 0.5, 0.8, 1.0$ and $\omega_E/t = 1.0$ while the total coupling strength is kept fixed: $V_R + V_D = t$. Exact numerical results are compared with those from the Momentum Average (MA) method. Agreement is excellent. Strong coupling results are also plotted (in red) by utilizing the Lang-Firsov (LF) strong coupling approximation. Agreement in the strong coupling regime ($\lambda \geq 1$) is excellent. (b) Effective mass m^*/m_{SO} vs. λ. MA results are plotted (symbols) with the exact numerical results, and again, agreement is excellent. In both (a) and (b) the polaronic effects are minimized for $V_R = V_D$.
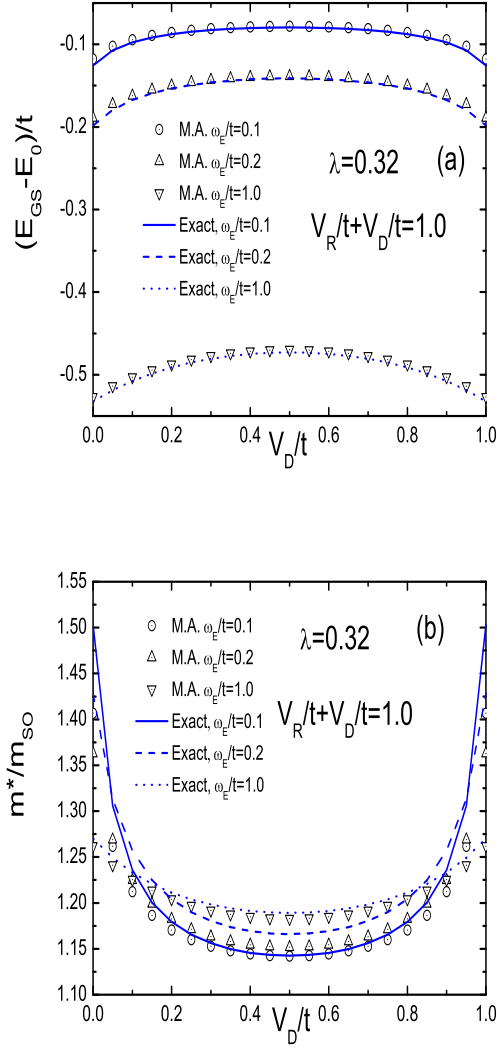
Figure 4.4: (a) Ground state energy $E_{GS} - E_0$ as a function of spin orbit coupling V_D/t for $\omega_E/t = 0.1, 0.2, 1.0$ with weak electron phonon coupling, $\lambda = 0.32$, and moderate spin-orbit coupling, $V_R + V_D = t$. (b) Effective mass m^*/m_{SO} as a function of spin orbit coupling V_D/t for the same parameters. MA results are again compared with the exact numerical results, and are reasonably accurate for these parameters.

$\lambda \geq 1$ regime. Similarly, weak coupling perturbation theory (Li et al., 2011) agrees with the exact results for $\lambda \leq 1$ (not shown). Fig. 4.3(b) shows the effective mass as a function of coupling strength; it decreases slightly, for a given value of λ, by increasing V_D in lieu of V_R.

All these results are plotted as a function of the electron phonon coupling strength, λ, as defined above; this definition requires the value of the electron density of states at the bottom of the band, and we have elected to use, for any value of spin-orbit coupling, the value $1/(4\pi t)$ appropriate to *no* spin-orbit coupling. If the actual DOS appropriate to the value of spin-orbit coupling were used in the definition of λ, then the effective mass, for example, would vary even more with varying V_D vs. V_R (see Fig. 2(b)). Moreover, this variation would be more pronounced for lower values of ω_E.

In Fig. 4.4, we show results for the ground state energy and effective mass for different values of the Einstein phonon frequency, ω_E; MA results are also shown for comparison. In these plots the electron phonon coupling strength is kept fixed and V_D is varied while maintaining the total spin-orbit coupling constant. The ground state energy has a maximum when the two spin-orbit coupling strengths, V_D and V_R, are tuned to be equal; similarly, the effective mass has a minimum when the two are equal. As the phonon frequency is reduced the minimum in the effective mass becomes more pronounced. The MA results track the exact results, and, as found previously (Li et al., 2011), are slightly less accurate as the phonon frequency becomes much lower than the hopping matrix element, t.

4.4 Chapter Summary

Linear spin-orbit coupling can arise in two varieties; taken on their own, they are essentially equivalent, and their impact on a single electron, even in the presence of electron phonon interactions, will be identical. However, with the ability to tune either coupling constant, in both solid state and cold atom experiments, one can probe the degree of Dresselhaus vs. Rashba spin-orbit coupling, through the impact on polaronic properties. The primary effect of this variation is the electron density of states, where the van Hove singularity can be moved as a function of chemical potential (i.e. doping) through tuning of the spin-orbit parameters. These conclusions are based on exact methods (the so-called Trugman method), and are not subject to approximations. These results have been further corroborated and understood through the Momentum Average approximation, and through weak and strong coupling perturbation theory. The effect is expected to be experimentally relevant since in typical materials with large spin-orbit couplings the phonon frequency is small when compared to the bandwidth, $\omega_E/t \ll 1$.

CHAPTER 5

Su-Schrieffer-Heeger Polaron [1]

5.1   Introduction

When electrons interact strongly with phonons, the electrons acquire a polaronic character, i.e. they move around the lattice much more sluggishly than non-interacting electrons would, because a polarization cloud must accompany them as they move. A measure of the strength of the coupling between the electron and the phonons is the degree to which the ground state energy is lowered. For example, previous studies for the Holstein model (Holstein, 1959a,b) have indicated that the decrease in energy is proportional to the bare coupling strength (λ) in strong coupling (Marsiglio, 1995), independent of the value of the phonon frequency. On the other hand, in weak coupling, while the proportionality to λ remains, there is some dependence on phonon frequency, and in fact, the decrease in energy is greater for higher phonon frequency (Marsiglio, 1995; Li et al., 2010).

A much more indicative measure of the polaronic character of an electron is the effective mass. In the Holstein model a glimpse of polaronic tendencies, even within

---

[1]A version of this chapter has been published. Zhou Li et.al, 2011, Phys. Rev. B 83, 045104.

perturbation theory, can be attained by examining the effective mass, particularly in one dimension. Usually an increasing effective mass is accompanied by a decrease in quasiparticle residue, although this is not always the case, as described below.

The Holstein model describes electrons interacting with optical phonons; the coupling is via the electron charge density, and, in this sense, the Holstein model serves as a paradigm for electron-phonon interactions just like the celebrated Hubbard model (Hubbard, 1963, 1964) is the simplest description of electron-electron interactions. Many of the basic features of this model are now fairly well understood — see Fehske and Trugman (2007) and Alexandrov (2007) along with more recent work in Li et al. (2010) and Alvermann et al. (2010). However, just as important is the electron interaction with acoustic phonons; typically the ionic motions couple to the electron motion, as opposed to its charge density. A very simple model to describe this kind of electron-phonon interaction within a tight-binding framework is given by

$$
\begin{aligned}
H &= -\sum_{\langle i,j \rangle} t_{ij} \left(c_{i\sigma}^{\dagger} c_{j\sigma} + h.c. \right) + \sum_{i} \left[\frac{p_{xi}^2}{2M} + \frac{p_{yi}^2}{2M} \right] \\
&+ \frac{1}{2} K \sum_{\langle i,j \rangle} \left[\left(u_{xi} - u_{xj} \right)^2 + \left(u_{yi} - u_{yj} \right)^2 \right],
\end{aligned}
\tag{5.1}
$$

where angular brackets denote nearest neighbours only, and

$$
t_{ij} = t - \alpha(u_{xi} - u_{xj})\delta_{i,j\pm\hat{a}_x} - \alpha(u_{yi} - u_{yj})\delta_{i,j\pm\hat{a}_y}.
\tag{5.2}
$$

This Hamiltonian has been written specifically for two dimensions, but the generalization to three dimensions (or back to one dimension) is evident from Eqs. (5.1) and (5.2). The operators and parameters are as follows: $c_{i\sigma}^{\dagger}$ $(c_{i\sigma})$ creates (annihi-

lates) an electron at site i with spin σ. The x-components for the ion momentum and displacement are given by p_{xi}, and displacement u_{xi}, respectively (similarly for the y-components), and the ions have mass M and spring constant K connecting nearest neighbours only. The electron-ion coupling is linearized in the components of the displacement, and we choose to include only longitudinal coupling.

This Hamiltonian is commonly known as the Su-Schrieffer-Heeger (SSH) model (Su et al., 1979, 1980), because it was used for seminal work describing excitations in polyacetylene by these authors. However, it was also introduced and studied a decade earlier by Barišić, Labbé, and Friedel (Barišić et al., 1970; Barišić, 1972a,b) to describe superconductivity in transition metals, so we will refer to it as the BLF-SSH model. Much of the work done on this model is in the adiabatic approximation, i.e. the phonons are treated classically (Su et al., 1979, 1980). This was followed by an examination of quantum fluctuations through quantum Monte Carlo and renormalization group studies (Hirsch and Fradkin, 1982; Fradkin and Hirsch, 1983), and these authors focused on half-filling. They found that the lattice ordering (in one dimension) was reduced by quantum fluctuations.

Very little work has been done, however, in the quantum regime for a single electron. Capone and coworkers studied a model similar to this one, except that they utilized optical phonons instead of acoustic ones (Capone et al., 1997; Marchand et al., 2010). This leads to some significant differences, about which we will comment below. In the past decade Zoli has studied the BLF-SSH polaron using perturbation theory, and found, for example, a perturbative regime in one dimension where polaron effects are absent (Zoli, 2002). This result happened to agree with the conclusions of Capone et al (Capone et al., 1997). in the perturbative regime of the CSG model (Marchand et al., 2010). In this paper we focus on 2nd order perturbation theory, and find results in disagreement with Zoli (2002). These results also disagree *qualita-*

tively with the results from the CSG model. That is, in one dimension, for example, perturbation theory breaks down as the characteristic phonon frequency decreases. In two dimensions there is a modest mass enhancement for all characteristic phonon frequencies, while in three dimensions the mass enhancement approaches unity in the adiabatic limit. We also note that the quasiparticle residue does not necessarily follow the trend of the inverse effective mass, as the characteristic phonon frequency varies.

This chapter is organized as follows. In the following section we outline the calculation, both using perturbation theory, and using Green function techniques. For some of our work (especially in one dimension), the calculation can be done analytically, and we derive these results where applicable. In Section IV we show some numerical results and compare our results with previous work and other electron-phonon models. We close in the final section with a summary. The main conclusion is that, as far as one can tell from weak coupling perturbation theory, the BLF-SSH model has a stronger tendency to form a polaronic state than is the case with the Holstein model. In one dimension this is most evident in the effective mass, and not at all evident in the quasiparticle residue.

5.2   Perturbation theory

5.2.1   Hamiltonian

The Hamiltonian Eq. (5.1), Fourier-transformed to wavevector space, and utilizing phonon creation and annihilation operators, is written (again in 2D),

$$
\begin{aligned}
H \;=\;& \sum_{k\sigma} \epsilon_{k\sigma} c_{k\sigma}^{\dagger} c_{k\sigma} \\
+\;& \sum_{q} \hbar\omega(q)\big[a_{xq}^{\dagger}a_{xq} + a_{yq}^{\dagger}a_{yq}\big] \\
+\;& \sum_{\substack{kk' \\ \sigma}} g_x(k,k')\big[a_{xk-k'} + a_{x-(k-k')}^{\dagger}\big]c_{k\sigma}^{\dagger}c_{k'\sigma} \\
+\;& \sum_{\substack{kk' \\ \sigma}} g_y(k,k')\big[a_{yk-k'} + a_{y-(k-k')}^{\dagger}\big]c_{k\sigma}^{\dagger}c_{k'\sigma}.
\end{aligned}
\tag{5.3}
$$

Here,

$$
\epsilon_k \equiv \epsilon(k_x, k_y) = -2t[\cos{(k_x)} + \cos{(k_y)}]
\tag{5.4}
$$

is the dispersion relation for non-interacting electrons with nearest neighbour hopping, and

$$
\omega(q) \equiv \omega_0 \sqrt{\sin^2{(q_x/2)} + \sin^2{(q_y/2)}}
\tag{5.5}
$$

is the phonon dispersion for acoustic phonons with nearest neighbour spring constants K, and $\omega_0 \equiv \sqrt{4K/M}$ is the characteristic phonon frequency. The phonon creation and annihilation operators are given by $a_{xq}^{\dagger}$ and a_{xq}, respectively, and similarly for those in the y-direction. The coupling "constants" are given by

$$
g_x(k,k') \equiv i\alpha \sqrt{\frac{2}{MN\omega(k-k')}}\left[\sin{(k_x')} - \sin{(k_x)}\right],
\tag{5.6}
$$

with a similar expression for the y direction, and M is the mass of the ion and N is the number of lattice sites.

5.2.2 Green's function analysis

Carrying out a Green's function analysis using the free electron and phonon parts of the Hamitonian as the unperturbed part, gives, for the self energy of a single electron to lowest (2nd) order in the coupling α,

$$\Sigma(k, \omega + i\delta) =$$
$$-\sum_{k'} \big[|g_x(k, k')|^2 + |g_y(k, k')|^2 \big] G_0(k', \omega + i\delta - \omega(k - k')), \tag{5.7}$$

where $G_0(k, \omega + i\delta) \equiv \big[\omega + i\delta - \epsilon_k \big]^{-1}$ is the non-interacting electron retarded propagator.

One way to determine the effect of interactions on the electron dispersion is to compute the renormalized energy for the ground state (here, $k_x = k_y = 0$), and the effective mass. The effective mass has long been used as the primary indicator for polaronic behaviour (Fehske and Trugman, 2007; Alexandrov, 2007), and though within 2nd order perturbation we can only get an indication of this crossover, we use it here nonetheless. The renormalized energy is given by the solution for the pole location in the interacting electron Green's function, $G(k, \omega + i\delta) \equiv \big[\omega + i\delta - \epsilon_k - \Sigma(k, \omega + i\delta) \big]^{-1}$,

$$E_k = \epsilon_k + \text{Re}\Sigma(k, E_k). \tag{5.8}$$

To determine the effective mass, defined by the expectation that $E_k \equiv \hbar^2 k^2 / (2m^*)$, we take two derivatives of Eq. (5.8), and, using the fact that $(dE_k/dk)|_{k=0} = 0$, we

obtain

$$
\begin{aligned}
\frac{m^*}{m} &= \frac{1 - \frac{\partial \Sigma(k,\omega)}{\partial \omega}|_{\omega=E_k}}{1 + \frac{1}{2t}\frac{\partial^2 \Sigma(k,\omega)}{\partial k^2}|_{\omega=E_k}} \\
&= 1 - \frac{\partial \Sigma(k,\omega)}{\partial \omega}|_{\omega=E_k} - \frac{1}{2t}\frac{\partial^2 \Sigma(k,\omega)}{\partial k^2}|_{\omega=E_k}.
\end{aligned}
\tag{5.9}
$$

Here we have used the fact that the band mass given by the electron dispersion in Eq. (5.4) is $m = 1/(2t)$. Note that it is common (and advisable) to replace the substitutions for ω required in Eq. (5.9) with ϵ_k, rather than with E_k. This is due to the fact that the former substitution keeps the evaluation for every term at $O(\alpha^2)$, whereas the latter substitution includes some (inconsistently) higher order contributions. The former substitution is known as Rayleigh-Schrodinger perturbation theory while the latter is known as Brillouin-Wigner perturbation theory (Mahan, 2000). This means that we will use the following equation,

$$
\frac{m^*}{m} = 1 - \frac{\partial \Sigma(k,\omega)}{\partial \omega}|_{\omega=\epsilon_k} - \frac{1}{2t}\frac{\partial^2 \Sigma(k,\omega)}{\partial k^2}|_{\omega=\epsilon_k},
\tag{5.10}
$$

to define the effective mass.

In contrast the quasiparticle residue is defined as the weight that remains in the δ-function-like portion of the spectral weight. The spectral weight is defined as

$$
\begin{aligned}
A(k,\omega) &\equiv -\frac{1}{\pi}\mathrm{Im}G(k,\omega+i\delta) \\
&= -\frac{1}{\pi}\mathrm{Im}\frac{1}{\omega+i\delta-\epsilon_k-\Sigma(k,\omega+i\delta)}.
\end{aligned}
\tag{5.11}
$$

For a given momentum, as the energy of the pole given by Eq. (5.8) is approached, the imaginary part of the self energy tends towards zero; this produces a δ-function

contribution in Eq. (5.11) , at the pole energy, but with weight z_k defined by

$$z_k = \frac{1}{1 - \frac{\partial \Sigma(k,\omega)}{\partial \omega}|_{\omega=E_k}}. \tag{5.12}$$

The relationship amongst these various quantities — effective mass in Eq. (5.9), effective mass in Eq. (5.10), and quasiparticle residue in Eq. (5.12) — is discussed further in Appendix D.

5.2.3 Standard perturbation theory

Eq. (5.9) requires a numerical evaluation of Eq. (5.7), and then the required derivatives can be (numerically) determined. Because the positions of the singularities in Eq. (5.7) are difficult to determine in advance, it is customary to introduce a small (numerical) imaginary part corresponding to the infinitesimal δ, and then the numerical integration is more stable. This trick remains problematic, as we discuss further below. Alternatively, we can simply perform a 2nd order perturbation theory expansion, as outlined in every undergraduate quantum mechanics textbook. The result is

$$E_k^{(2)} = \frac{2\alpha^2}{M} \frac{1}{N} \sum_{k'} \frac{\left(\sin k'_x - \sin k_x\right)^2 + \left(\sin k'_y - \sin k_y\right)^2}{\omega(k - k') \quad [\epsilon_k - \epsilon_{k'} - \omega(k - k')]}, \tag{5.13}$$

where we remember that the first order (in α) contribution is of course zero, and the superscript (2) indicates the 2nd order contribution. Comparison with Eq. (5.7) shows that this corresponds to Rayleigh-Schrodinger perturbation theory with the self energy, evaluated at $\omega = \epsilon_k$ corresponding to the 2nd order energy correction. Eq. (5.13) can be evaluated numerically, and then two derivatives with respect to k are required. However, the same numerical problems mentioned above will arise;

fortunately, at least in one dimension, Eq. (5.13) can be evaluated analytically, whereas we were unable to do the same with Eq. (5.7).

5.3 Results and Discussion

5.3.1 Analytical results in 1D

The result of an analytical evaluation of Eq. (5.13) is, in one dimension,

$$E^{(2)}(k) = -\frac{32t}{\pi}\lambda_{\text{BLF}}\tilde{\omega}_0\left\{-2\cos k + \pi\tilde{\omega}_0 + C_k(\tilde{\omega}_0)\right\}, \qquad (5.14)$$

where $\tilde{\omega}_0 \equiv \omega_0/(4t)$, and a dimensionless coupling parameter λ_{BLF} is defined, in analogy to the dimensionless coupling parameter defined in the Holstein model, as

$$\lambda_{\text{BLF}} \equiv \frac{\alpha^2}{M\omega_0^2}\frac{1}{W}, \qquad (5.15)$$

where here the bandwidth $W = 4t$ for one dimension. Note that this coupling parameter has nothing to do physically with the coupling parameter defined in the Holstein model, so we will treat them as completely independent. The function $C_k(\tilde{\omega}_0)$ must be evaluated separately in the two regimes:

$$C_k(\tilde{\omega}_0) = 2\sqrt{\tilde{\omega}_0^2 - 1}\left(h(k) + h(-k) - 2h(\pi/2)\right), \quad \tilde{\omega}_0 > 1, \qquad (5.16)$$

where

$$h(k) = \tan^{-1}\left(\frac{\tilde{\omega}_0\tan\frac{k}{2} + 1}{\sqrt{\tilde{\omega}_0^2 - 1}}\right) \qquad (5.17)$$

and

$$C_k(\tilde{\omega}_0) = \sqrt{1 - \tilde{\omega}_0^2}\left(s(k) + s(-k) - 2s(\pi/2)\right), \quad \tilde{\omega}_0 < 1, \qquad (5.18)$$

where

$$s(k) = \log\left(\frac{\tilde{\omega}_0 \tan\frac{k}{2} + 1 + \sqrt{1 - \tilde{\omega}_0^2}}{\tilde{\omega}_0 \tan\frac{k}{2} + 1 - \sqrt{1 - \tilde{\omega}_0^2}}\right). \tag{5.19}$$

Eq. (5.14) is readily evaluated at $k = 0$ to determine the ground state energy. Evaluating the second derivative with respect to wave vector k is equally straightforward, and determination at $k = 0$ yields the rather simple result for the effective mass,

$$\frac{m^*}{m} = 1 + \frac{32}{\pi} \frac{\lambda_{\mathrm{BLF}}}{\tilde{\omega}_0}, \tag{5.20}$$

valid for all values of $\tilde{\omega}_0$.

5.3.2 Comparison with other models

An analytical result is readily available for the Holstein model; there, the ground state energy (in 1D) was given by(Marsiglio, 1995)

$$E_{\mathrm{H}} = -2t\left(1 + \lambda_{\mathrm{H}}\sqrt{\frac{\tilde{\omega}_E}{\tilde{\omega}_E + 1}}\right), \tag{5.21}$$

where $\tilde{\omega}_E \equiv \omega_E/(4t)$ is the Einstein phonon frequency normalized to the bandwidth, and, as explained earlier, the dimensionless coupling constant λ_{H} cannot be compared directly to the corresponding quantity for the BLF-SSH model. The effective mass is given by

$$\left(\frac{m^*}{m}\right)_{\mathrm{H}} = 1 + \frac{\lambda_{\mathrm{H}}}{4\sqrt{\tilde{\omega}_E}} \frac{1 + 2\tilde{\omega}_E}{\left(1 + \tilde{\omega}_E\right)^{3/2}}. \tag{5.22}$$

In both cases, as the characteristic phonon frequency approaches zero (adiabatic limit) the ground state energy approaches the non-interacting value; however, the effective mass diverges in this same limit. So, while the first statement would appear to justify perturbation theory in this limit, the second statement clearly indicates a breakdown in the adiabatic limit. It is known in both cases that the adiabatic

approximation leads to a polaron-like solution for all coupling constants (Kabanov and Mashtakov, 1993), and clearly these two observations are consistent with one another. In fact, the divergence is stronger in the BLF-SSH model, and goes beyond the inverse square-root behaviour observed for the Holstein model and attributed to the diverging electron density of states in one dimension (Capone et al., 1997); this indicates that the BLF-SSH model, at least in the adiabatic limit in one dimension, has a stronger tendency for polaron formation than the Holstein model.

Interestingly, in the model studied by Capone et al. (Capone et al., 1997), where optical phonons were used, the opposite behaviour was obtained; they found that the effective mass ratio approached unity as the characteristic phonon energy approached zero. In the opposite limit Capone et al. (Capone et al., 1997) found an effective mass ratio that did not approach unity as the characteristic phonon frequency increased (anti-adiabatic limit). In the BLF-SSH model, however, this ratio does approach unity as the phonon frequency increases beyond the electron bandwidth, in one dimension, in agreement with the Holstein result in all dimensions. As we will see below, however, in the BLF-SSH model in two and three dimensions the effective mass ratio remains above unity in the anti-adiabatic limit. This is not surprising, since here the interaction modulates the hopping, and we expect a non-zero correction in this limit. In the adiabatic limit, the BLF-SSH mass ratio approaches a constant value in two dimensions, and falls to unity in three dimensions, both in agreement with the behaviour in the Holstein model.

Our results disagree with those of Zoli (2002) for reasons that are not entirely clear. We have utilized both the straightforward perturbation theory method (analytically and numerically), and the Green's function formalism (numerically). In the latter case we required a numerically small imaginary part for the frequency significantly smaller than the value quoted in Zoli (2002) (we used $\delta = 10^{-9}$ whereas he used
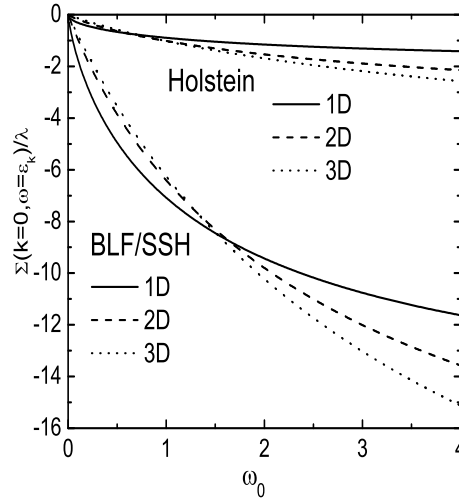
Figure 5.1: Electron self energy for the ground state $(k = 0)$, normalized to λ (or λ_H) vs. characteristic phonon frequency ω_0 (this is ω_E for the Holstein model), for both the BLF-SSH and Holstein models, in one, two, and three dimensions, as indicated. Alternatively, the ordinate is simply the second order (in g) correction to the ground state energy within Rayleigh-Schrodinger perturbation theory. In all cases the magnitude of the correction increases with increasing ω_0. The 1D (3D) result has highest magnitude at low (high) frequency. All six cases have non-zero limiting values as $\omega_0 \to \infty$, given in Table 1.

$\delta = 10^{-4}$. However, as is clear from our analytical result, Eq. (5.20), our effective mass diverges at low phonon frequency, and decreases monotonically to unity as the phonon frequency increases. The result in Zoli (2002) peaks sharply near $\tilde{\omega}_0 \approx 1$, and, as noted above, decreases to unity at low phonon frequency.

5.3.3   Numerical results

In Fig. 5.1 we plot the reduction in the ground state energy due to the second order correction (for the BLF-SSH model, this is given by Eq. (5.13)), normalized to λ

(or λ_H). This is also written as $\Sigma(k=0, \omega = \epsilon_k)/\lambda$, where the self energy is given by the expression in Eq. (5.7). Also plotted for comparison are the corresponding quantities for the Holstein model. Note that both models share a few features in common: (i) they both go to zero as the characteristic phonon energy decreases to zero, regardless of the dimensionality, (ii) they all approach a non-zero negative (and finite) value as the characteristic phonon frequency grows, and (iii) they cross one another in strength as a function of dimensionality as ω_0 increases, i.e. at low phonon frequencies the self energy has the highest magnitude for one dimension, whereas for high phonon frequency the highest magnitude is achieved in both models for three dimensional systems. Also note that the BLF-SSH results are well separated from Holstein results. In particular, there appears to be more 'bang for the buck' with the BLF-SSH model, i.e. for a given value of λ and the same characteristic phonon frequency, the energy reduction is almost an order of magnitude higher for the BLF-SSH model as compared with the Holstein model. Again, we remind the reader that the value of λ in the Holstein model has nothing to do with the value of λ in the BLF-SSH model, so this comparison is unwarranted.

For this reason we will use the value for the self energy, in weak coupling, as the phonon frequency increases to infinity, as the energy scale that provides a measure of the energy lowering expected for a given model and a given dimensionality. These numbers, mostly determined analytically, are provided in Table I.

Table 5.1: $\lim_{\omega_0 \to \infty} \Sigma(k=0, \omega = \epsilon_k)/(\lambda t)$

Dim.	BLF-SSH	Holstein
1D	-16	-2
2D	-23.3	-4
3D	-30.2	-6

In Fig. 5.2 we plot the effective mass ratio (minus unity), normalized to the self
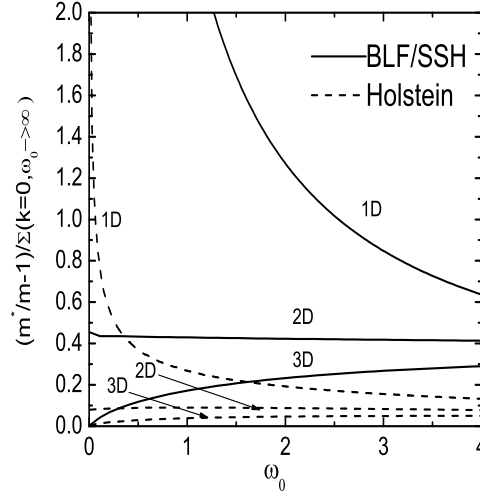
Figure 5.2:   The electron effective mass, normalized to the 2nd order correction to the energy for the anti-adiabatic limit, vs. characteristic phonon frequency, ω_0, for both the BLF-SSH and Holstein models, in one, two, and three dimensions, as indicated. In 1D the effective mass diverges for both models, though the divergence is stronger for the BLF-SSH model, as indicated by Eq. (5.20). In 2D the effective mass approaches a constant as $\omega_0 \to 0$ for both models, while in 3D the effective mass ratio approaches unity in the same limit. At the opposite extreme, both 1D results give $m^*/m \to 1$ as $\omega_0 \to \infty$, while in both 2D and 3D the effective mass remains above unity in this limit. Note that in all three dimensions, for a given reduction in energy as given by the 2nd order correction to the energy, the BLF-SSH model results in significantly higher effective masses.

energy evaluated for infinite characteristic phonon frequency. This normalization is important to divide out enhancements that are solely due to definitions. Moreover, in this way, we are determining the mass enhancement for a given 'coupling strength', where this strength is now a measure of the energy lowering caused by a certain amount of coupling to phonons, regardless of the origin of that coupling. This plot now makes clear that the BLF-SSH model, within weak coupling perturbation theory, has more 'polaronic' tendency than the Holstein model. Note in particular
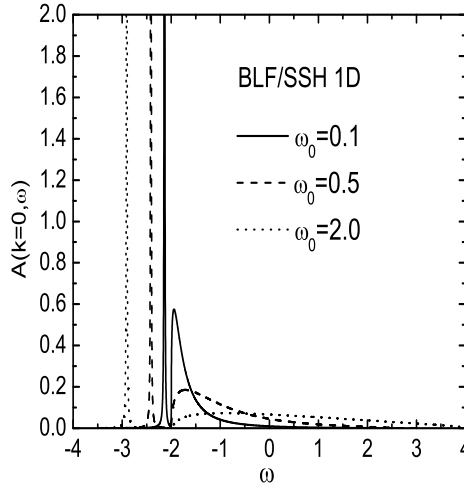
Figure 5.3: Spectral function for the BLF-SSH model, for $\lambda = 0.2$ for three different characteristic phonon frequencies, as a function of frequency. All three spectra are similar as one would find for the Holstein model, and consist of quasiparticle peak with weight $z_0 = 0.766, 0.727, 0.724$, for $\omega_0/t = 0.1, 0.5, 2.0$, respectively, followed by an incoherent piece.

that the divergence (in 1D) at low characteristic phonon frequency is much stronger for the BLF-SSH model, as Eq. (5.20) already indicated. Thus, as discussed above, we anticipate that in the adiabatic approximation, in 1D, the system will always be polaronic, regardless of the coupling strength, in agreement with the result of the Holstein model (Kabanov and Mashtakov, 1993), and in disagreement with the result from the hybrid model defined in Capone et al. (1997).

Otherwise, the behaviour of the effective mass in the two models is very similar, as a function of characteristic phonon frequency, for the various dimensions shown. The effective mass can be made arbitrarily close to unity, for any non-zero phonon frequency, for sufficiently weak coupling. Preliminary numerical calculations indicate a free electron-like to polaron crossover (Li et al.; Chandler and Marsiglio) similar
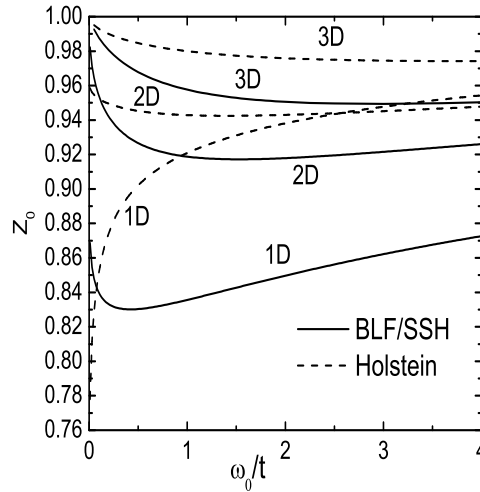
Figure 5.4:   Quasiparticle residue, z_0 vs. ω_0/t for both the BLF-SSG and Holstein models. in all three dimensions. Note that while the result for the Holstein model tends to be inversely proportional to the effective mass, this is not the case for the BLF-SSh model at low phonon frequency, and in 1D and 2D. In one dimension in particular, the effective mass diverges, while z_0 also turns upward.

to what was found for the Holstein model.

5.3.4   Spectral function

It is interesting to examine the spectral function, defined by Eq. (5.11) (see also the discussion in the Appendix). For simplicity we show the result in one dimension, in Fig. 5.3, for the ground state ($k = 0$) as a function of frequency.

The results for two or three dimensions do not differ in any significant way from these results. The results for three different characteristic phonon frequencies are shown. In each case a quasiparticle δ-function is present (here artificially broadened so as to be visible), followed by an incoherent piece; the incoherent part has energies

ranging approximately from $-2t < \omega < +2t + \omega_0$. The quasiparticle residue, z_0 must be determined numerically, and is given in the figure caption for each of the cases considered (see also Fig. 5.4. We have verified that the remaining weight (the spectral functions each have weight unity) is present in the incoherent part. The result shown is not too different from what is found in the Holstein model; the singularities from the 1D electron density of states are now smeared out in the incoherent piece, as result of the coupling and phonon energy having some frequency dependence. We show in Fig. 5.4, as a function of ω_0, the quasiparticle residue for both the Holstein and BLF-SSH models. The Holstein results tend to follow the inverse of the result for the inverse effective mass; this is as expected. This is not the case with the BLF-SSH, but for more subtle reasons than the fact that the self energy is now momentum dependent. The more important effect, which shows up in both 1D and 2D results, is that the quasiparticle weight requires an evaluation of the frequency derivative of the self energy at the energy of the pole, whereas the effective mass in Rayleigh-Schrodinger perturbation theory requires the same derivative at the *non-interacting* ground state energy. Most noteworthy is that the quasiparticle residue show a clear upturn at low characteristic phonon frequencies, while the inverse effective mass clearly approaches zero (see Fig. 5.2) as this characteristic frequency is taken to zero.

To see this more clearly we show in Fig. 5.5 a comparison of the residue (upper panel) vs. effective mass (lower panel), as a function of ω_0, for two (weak) strengths of electron phonon coupling. At high phonon frequency, as the former decreases, the latter increases with decreasing phonon frequency, but at low phonon frequency, the two properties no longer behave in inverse fashion with respect to one another.
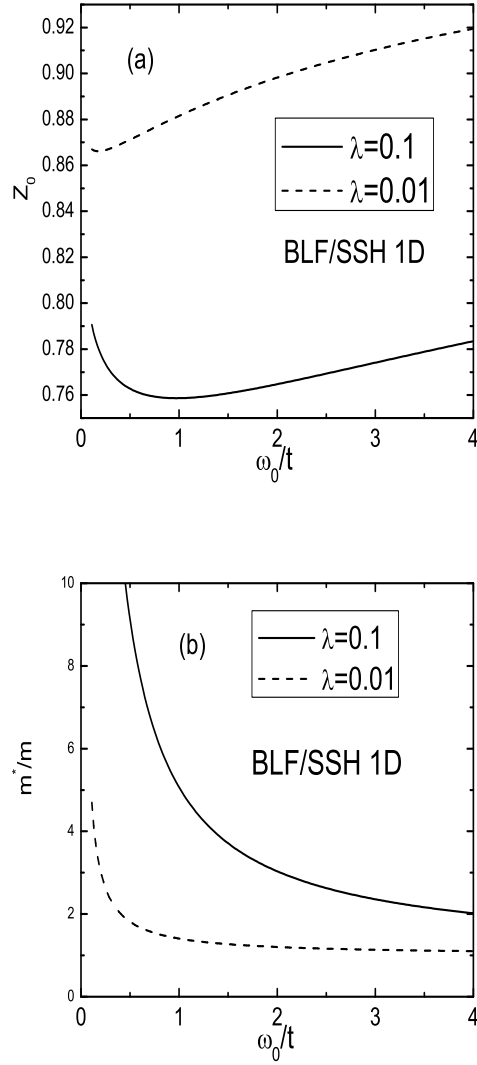
Figure 5.5: Comparison of the quasiparticle residue (upper panel) with the electron effective mass (lower panel) as a function of ω_0/t, for the BLF-SSH model in one dimension. The behaviour noted in Fig. 5.4 is clear here. Moreover, note the scales; while the effective mass ratio is very large (≈ 4) for $\lambda = 0.01$ and small values of ω_0/t, the quasiparticle residue remains within 15% of unity.

5.4 Chapter Summary

The BLF-SSH model appears to have very strong polaronic tendencies, stronger than those of, say, the Holstein model, especially in one dimension. This conclusion is based on the 2nd order perturbative calculation performed in this chapter, but also has corroborative evidence from calculations in the strong coupling regime. In one dimension we have been able to obtain an analytical solution for the ground state energy and the effective mass. The conclusion concerning polaronic behaviour is an important one, as much of what we know about polarons arises from Holstein-like models. In particular, for a coupling strength that leads to a fixed amount of energy lowering (in 2nd order), the effective mass can become an order of magnitude larger than the bare mass, a clear indicator that perturbation theory breaks down. This occurs in the BLF-SSH model at much weaker coupling than in the Holstein model. We have also noted that the relationship between effective mass and quasiparticle residue breaks down in one and two dimensions for the BLF-SSH model, not because of the momentum dependence in the self energy, but because the two properties involve evaluation of the frequency derivative of the self energy at different energies.

CHAPTER 6

Conclusion

In this thesis we have developed a numerical technique to study the electron-phonon interaction using various models (Holstein model, Rashba-Holstein model, Rashba-Dresselhaus-Holstein model and BLF-SSH model). We have established the weak coupling and the strong coupling regime in two dimensions and higher. We found that in the weak coupling regime the electron is nearly free while in the strong coupling regime the behavior of the electron can be described by the quasiparticle named a polaron. In the strong coupling regime there is also an analytical method using the Lang-Firsov transformation. We have obtained analytical results for the Holstein model, Rashba-Holstein model as well as for the Rashba-Dresselhaus-Holstein model in the strong coupling regime and found good agreement with the numerical results. For the BLF-SSH model the strong coupling regime remains difficult for both numerical and analytical methods. We have also studied the crossover from the weak coupling regime to the strong coupling regime. In one dimension the crossover is smooth, so the electron retains polaronic character for all values of electron-phonon interaction. In two dimensions and higher the crossover is sharp; and the crossover becomes sharper for low phonon frequency, that is, near the adiabatic limit.

We have also considered other kinds of interactions, for example, the spin-orbit interaction. The ground state will be greatly modified by the spin-orbit interaction. So the effective mass and the ground state energy can be tuned by the spin-orbit interaction. We have also studied the non-interacting density of states and found the Van-Hove singularities will be shifted away from the bottom of the band as the spin-orbit interaction increases. These effects can be possibly observed in the cold atom experiments (Lin et al., 2011; Herrera and Krems, 2011).

For the BLF-SSH model, we have found a divergence of effective mass near the adiabatic limit in one dimension. This is similar as what happens for the Holstein model. But the divergence will go as $1/\omega_E$ for BLF-SSH model compared to $1/\sqrt{\omega_E}$ for Holstein model. We have also found an unusual relationship between the spectral weight and the effective mass.

Bibliography

Alexandrov, A. S. "Breakdown of the Migdal-Eliashberg theory in the strong-coupling adiabatic regime." *EPL (Europhysics Letters)* 56 (2001): 92.

Alexandrov, A. S. "Polarons in Advanced Materials Springer Series in Material Sciences." 103 (2007): 257–310.

Alexandrov, A. S., V. V. Kabanov, and D. K. Ray. "From electron to small polaron: An exact cluster solution." *Phys. Rev. B* 49 (Apr 1994): 9915–9923.

Alexandrov, A.S. and N. Mott. "Polarons and Bipolarons." (1995).

Alvermann, Andreas, Holger Fehske, and Stuart A. Trugman. "Polarons and slow quantum phonons." *Phys. Rev. B* 81 (Apr 2010): 165113.

Anderson, M. H., J. R. Ensher, M. R. Matthews, C. E. Wieman, and E. A. Cornell. "Observation of Bose-Einstein Condensation in a Dilute Atomic Vapor." *Science* 269 (1995): 198–201.

Anderson, P. W. "The Resonating Valence Bond State in La2CuO4 and Superconductivity." *Science* 235 (1987): 1196–1198.

Anderson, P. W. and Elihu Abrahams. "Superconductivity theories narrow down." *Nature* 327 (1987): 363.

Ast, Christian R., Jürgen Henk, Arthur Ernst, Luca Moreschini, Mihaela C. Falub, Daniela Pacilé, Patrick Bruno, Klaus Kern, and Marco Grioni. "Giant Spin Splitting through Surface Alloying." *Phys. Rev. Lett.* 98 (May 2007): 186807.

Ast, Christian R., Gero Wittich, Peter Wahl, Ralf Vogelgesang, Daniela Pacilé, Mihaela C. Falub, Luca Moreschini, Marco Papagno, Marco Grioni, and Klaus Kern. "Local detection of spin-orbit splitting by scanning tunneling spectroscopy." *Phys. Rev. B* 75 (May 2007): 201401.

Bardeen, J. "Zero-Point Vibrations and Superconductivity." *Phys. Rev.* 79 (Jul 1950): 167–168.

Bardeen, J., L. N. Cooper, and J. R. Schrieffer. "Microscopic Theory of Superconductivity." *Phys. Rev.* 106 (Apr 1957): 162–164.

Bardeen, J., L. N. Cooper, and J. R. Schrieffer. "Theory of Superconductivity." *Phys. Rev.* 108 (Dec 1957): 1175–1204.

Barišić, S. "Rigid-Atom Electron-Phonon Coupling in the Tight-Binding Approximation.I." *Phys. Rev. B* 5 (Feb 1972): 932–941.

Barišić, S. "Self-Consistent Electron-Phonon Coupling in the Tight-Binding Approximation. II." *Phys. Rev. B* 5 (Feb 1972): 941–951.

Barišić, S., J. Labbé, and J. Friedel. "Tight Binding and Transition-Metal Superconductivity." *Phys. Rev. Lett.* 25 (Oct 1970): 919–922.

Bednorz, J. G. and K. A. Müller. "Possible high Tc superconductivity in the Ba-La-Cu-O system." 10.1007/BF01303701. *Zeitschrift für Physik B Condensed Matter* 64 (1986): 189–193.

Bednorz, J. Georg and K. Alex Müller. "Perovskite-type oxides–The new approach to high-T_c superconductivity." *Rev. Mod. Phys.* 60 (Jul 1988): 585–600.

Berciu, Mona. "Green's Function of a Dressed Particle." *Phys. Rev. Lett.* 97 (Jul 2006): 036402.

Bernevig, B. Andrei, J. Orenstein, and Shou-Cheng Zhang. "Exact SU(2) Symmetry and Persistent Spin Helix in a Spin-Orbit Coupled System." *Phys. Rev. Lett.* 97 (Dec 2006): 236601.

Bimberg, Dieter, Marius Grundmann, and Nikolai N. Ledentsov *Quantum Dot Heterostructures* (1999).

Bloch, Immanuel, Jean Dalibard, and Wilhelm Zwerger. "Many-body physics with ultracold gases." *Rev. Mod. Phys.* 80 (Jul 2008): 885–964.

Bonča, J., S. A. Trugman, and I. Batistić. "Holstein polaron." *Phys. Rev. B* 60 (Jul 1999): 1633–1642.

Capone, M., W. Stephan, and M. Grilli. "Small-polaron formation and optical absorption in Su-Schrieffer-Heeger and Holstein models." *Phys. Rev. B* 56 (Aug 1997): 4484–4493.

Cappelluti, E., C. Grimaldi, and F. Marsiglio. "Electron-phonon effects on spin-orbit split bands of two-dimensional systems." *Phys. Rev. B* 76 (Aug 2007): 085334.

Cappelluti, E., C. Grimaldi, and F. Marsiglio. "Topological Change of the Fermi Surface in Low-Density Rashba Gases: Application to Superconductivity." *Phys. Rev. Lett.* 98 (Apr 2007): 167002.

Chandler, C. and F. Marsiglio (unpublished).

Chen, Lei, Zhongshui Ma, J. C. Cao, T. Y. Zhang, and Chao Zhang. "Phonon-limited mobility in two-dimensional semiconductors with spin-orbit coupling." *Applied Physics Letters* 91 (2007): 102115.

Covaci, Lucian and Mona Berciu. "Polaron Formation in the Presence of Rashba Spin-Orbit Coupling: Implications for Spintronics." *Phys. Rev. Lett.* 102 (May 2009): 186403.

Dagotto, Elbio. "Correlated electrons in high-temperature superconductors." *Rev. Mod. Phys.* 66 (Jul 1994): 763–840.

Davis, K. B., M. O. Mewes, M. R. Andrews, N. J. van Druten, D. S. Durfee, D. M. Kurn, and W. Ketterle. "Bose-Einstein Condensation in a Gas of Sodium Atoms." *Phys. Rev. Lett.* 75 (Nov 1995): 3969–3973.

Dresselhaus, G *Phys. Rev.* (1955): 580–586.

Fehske, H. and S. A. Trugman. "Polarons in Advanced Materials Springer Series in Material Sciences." 103 (2007): 393–461.

Fradkin, Eduardo and Jorge E. Hirsch. "Phase diagram of one-dimensional electron-phonon systems. I. The Su-Schrieffer-Heeger model." *Phys. Rev. B* 27 (Feb 1983): 1680–1697.

Fröhlich, H. "Theory of the Superconducting State. I. The Ground State at the Absolute Zero of Temperature." *Phys. Rev.* 79 (Sep 1950): 845–856.

Greiner, Markus, Cindy A. Regal, and Deborah S. Jin. "Emergence of a molecular Bose-Einstein condensate from a Fermi gas." *Nature* (2003).

Grimaldi, C. "Large polaron formation induced by Rashba spin-orbit coupling." *Phys. Rev. B* 81 (Feb 2010): 075306.

Grimaldi, C., E. Cappelluti, and F. Marsiglio. "Off-Fermi surface cancellation effects in spin-Hall conductivity of a two-dimensional Rashba electron gas." *Phys. Rev. B* 73 (Feb 2006): 081303.

Grimaldi, C., E. Cappelluti, and F. Marsiglio. "Spin-Hall Conductivity in Electron-Phonon Coupled Systems." *Phys. Rev. Lett.* 97 (Aug 2006): 066601.

Haydock, R, V Heine, and M J Kelly. "Electronic structure based on the local atomic environment for tight-binding bands." *Journal of Physics C: Solid State Physics* 5 (1972): 2845.

Haydock, R, V Heine, and M J Kelly. "Electronic structure based on the local atomic environment for tight-binding bands. II." *Journal of Physics C: Solid State Physics* 8 (1975): 2591.

Herrera, Felipe and Roman V. Krems. "Tunable Holstein model with cold polar molecules." *Phys. Rev. A* 84 (Nov 2011): 051401.

Hirsch, J. E. "The True Colors of Cuprates." *Science* 295 (2002): 2226–2227.

Hirsch, Jorge E. and Eduardo Fradkin. "Effect of Quantum Fluctuations on the Peierls Instability: A Monte Carlo Study." *Phys. Rev. Lett.* 49 (Aug 1982): 402–405.

Holstein, T. "Studies of polaron motion: Part I. The molecular-crystal model." *Annals of Physics* 8 (1959): 325 – 342.

Holstein, T. "Studies of polaron motion: Part II. The small polaron." *Annals of Physics* 8 (1959): 343 – 389.

Hubbard, J. "Electron Correlations in Narrow Energy Bands." *Proceedings of*

the Royal Society of London. Series A. Mathematical and Physical Sciences 276 (1963): 238–257.

Hubbard, J. "Electron Correlations in Narrow Energy Bands. II. The Degenerate Band Case." *Proceedings of the Royal Society of London. Series A. Mathematical and Physical Sciences* 277 (1964): 237–259.

Kabanov, V. V. and O. Yu. Mashtakov. "Electron localization with and without barrier formation." *Phys. Rev. B* 47 (Mar 1993): 6060–6064.

Koralek, J. D., C. P. Weber, J. Orenstein, B. A.Bernevig, Shou-Cheng Zhang, S. Mack, and D. D. Awschalom. "Emergence of the persistent spin helix in semiconductor quantum wells." *Nature* 458 (2009): 610–613.

Ku, Li-Chung, S. A. Trugman, and J. Bonča. "Dimensionality effects on the Holstein polaron." *Phys. Rev. B* 65 (Apr 2002): 174306.

Lagendijk, Ad and Hans De Raedt. "On self-trapping in the molecular crystal model in onw, two and three dimensions." *Physics Letters A* 108 (1985): 91 – 94.

Lang, I. G. and Yu. A. Firsov *Sov. Phys. JETP* 16 (1963): 1301.

Li, Zhou, D. Baillie, C. Blois, and F. Marsiglio. "Ground-state properties of the Holstein model near the adiabatic limit." *Phys. Rev. B* 81 (Mar 2010): 115114.

Li, Zhou, C. Chandler, and F. Marsiglio (unpublished).

Li, Zhou, L. Covaci, M. Berciu, D. Baillie, and F. Marsiglio. "Impact of spin-orbit coupling on the Holstein polaron." *Phys. Rev. B* 83 (May 2011): 195104.

Li, Zhou, Zhongshui Ma, A. R. Wright, and Chao Zhang. "Spin-orbit interaction enhanced polaron effect in two-dimensional semiconductors." *Applied Physics Letters* 90 (2007): 112103.

Lin, Y. J., K. Jimenez-Garcia, and I. B. Spielman *Nature* (2011): 83.

Löwen, H. "Absence of phase transitions in Holstein systems." *Phys. Rev. B* 37 (May 1988): 8661–8667.

Mahan, G.D. "Many-Particle Physics." (2000).

Maiti, S.K., S. Sil, and A. Chakrabarti *arXiv:1109.5842v2* (2011).

Marchand, D. J. J., G. De Filippis, V. Cataudella, M. Berciu, N. Nagaosa, N. V. Prokof'ev, A. S. Mishchenko, and P. C. E. Stamp. "Sharp Transition for Single Polarons in the One-Dimensional Su-Schrieffer-Heeger Model." *Phys. Rev. Lett.* 105 (Dec 2010): 266605.

Marsiglio, F. "Pairing in the Holstein model in the dilute limit." *Physica C: Superconductivity* 244 (1995): 21 – 34.

Meier, L., G. Salis, I. Shorubalko, S. Schön E. Gini, and K. Ensslin *Nature Physics* (2007): 650.

Mott, N.F. "Is there an explanation?." *Nature* 327 (1987): 185.

Pacilé, D., C. R. Ast, M. Papagno, C. Da Silva, L. Moreschini, M. Falub, Ari P. Seitsonen, and M. Grioni. "Electronic structure of an ordered PbMAg(111) surface alloy: Theory and experiment." *Phys. Rev. B* 73 (Jun 2006): 245429.

Rashba, E.I. *Sov. Phys. Solid State* (1960): 1109.

Rotenberg, Eli, J. W. Chung, and S. D. Kevan. "Spin-Orbit Coupling Induced Surface Band Splitting in Li/W(110) and Li/Mo(110)." *Phys. Rev. Lett.* 82 (May 1999): 4066–4069.

Sakurai, J. J. "Advanced Quantum Mechanics." (1967).

Su, W. P., J. R. Schrieffer, and A. J. Heeger. "Solitons in Polyacetylene." *Phys. Rev. Lett.* 42 (Jun 1979): 1698–1701.

Su, W. P., J. R. Schrieffer, and A. J. Heeger. "Soliton excitations in polyacetylene." *Phys. Rev. B* 22 (Aug 1980): 2099–2111.

Trugman, S. A. "Applications of Statistical and Field Theory Methods to Condensed Matter." (1990).

Winkler, R. "Spin-Orbit Coupling Effects in Two-Dimensional Electron and Hole Systems." (2003).

Wolf, S. A., D. D. Awschalom, R. A. Buhrman, J. M. Daughton, S. von Molnr, M. L. Roukes, A. Y. Chtchelkanova, and D. M. Treger. "Spintronics: A Spin-Based Electronics Vision for the Future." *Science* 294 (2001): 1488–1495.

Y.Murayama *Mesoscopic Systems* (2001).

Zoli, Marco. "Mass renormalization in the Su-Schrieffer-Heeger model." *Phys. Rev. B* 66 (Jul 2002): 012303.

APPENDIX A

Trugman's method

The Trugman method is a variational method for electron-phonon coupled systems. Due to the fact that phonons are bosons, the Hilbert space will be infinite. The basis states in the whole Hilbert space will include two parts, the electron part and the phonon part. For one electron, the complicated structure of the basis states arises from the phonon part. Using the Holstein model in one dimension as an example, by applying the Hamiltonian to a specific basis state, one can generate at most four new states, which are the states with the electron hopping to the left, the electron hopping to the right, the phonon number increased by one and the phonon number decreased by one. Specifically, consider a state with six phonons on the same site of the electron

$$|\phi_n\rangle = \sum_j e^{ikR_j} c_j^\dagger (a_j^\dagger)^6 |0\rangle \tag{A.1}$$

and then apply the Hamiltonian to this state; we get

$$H|\phi_n\rangle = -t \sum_j e^{ikR_j} (c_{j+1}^\dagger + c_{j-1}^\dagger)(a_j^\dagger)^6 |0\rangle - g\omega_E \sum_j e^{ikR_j} c_j^\dagger [(a_j^\dagger)^7 + (a_j^\dagger)^5] |0\rangle. \tag{A.2}$$

By bringing the electron back to be at site j, we get

$$H|\phi_n\rangle = -t \sum_j e^{ikR_j} c_j^\dagger [e^{-ik}(a_{j-1}^\dagger)^6 + e^{ik}(a_{j+1}^\dagger)^6]|0\rangle - g\omega_E \sum_j e^{ikR_j} c_j^\dagger [(a_j^\dagger)^7 + (a_j^\dagger)^5]|0\rangle$$

The position of the phonons and the number of phonons at each site are stored in the program, so once a new state is generated, it will be compared to the old basis states. If that state is not already present, it will be added to the basis states. If we start from the bare electron state,

$$|\phi_0\rangle = \sum_j e^{ikR_j} c_j^\dagger |0\rangle, \tag{A.3}$$

by applying the Hamiltonian 20 times, we can get basis states with maximally 20 phonons. This is a truncation of the boson states and will make the program difficult to converge in the strong coupling limit. We have made refinements to this method to make it more flexible to deal with the truncation. The details of these refinements are in Chapter 2.

APPENDIX B

Notes for Chapter 1

B.1   Optical conductivity

We use the optical conductivity as an example,

$$\sigma_{\mu\nu}(\omega) = D\delta(\omega) + \sigma_{\mu\nu}^{reg}(\omega) \tag{B.1}$$

where D is the Drude weight at $\omega = 0$ and $\sigma^{reg}(\omega)$ is the regular part for $\omega > 0$ which can be calculated from Kubo's formula,

$$
\begin{aligned}
&\sigma_{\mu\nu}^{reg}(\omega) \\
&= \frac{1}{\omega} \int_0^\infty e^{i\omega t} dt \, \langle [j_\mu(t), j_\nu(0)] \rangle \\
&= \frac{1}{\omega} \int_0^\infty e^{i\omega t} dt \, \langle j_\mu(t) j_\nu(0) - j_\nu(0) j_\mu(t) \rangle \\
&= \frac{1}{\omega Z} \sum_{nn'} \left[\begin{array}{l} \int_0^\infty e^{i\omega t} dt \, \langle n | e^{iHt} j_\mu(0) e^{-iHt} | n' \rangle \langle n' | j_\nu(0) | n \rangle e^{-\beta E_n} \\ - \int_0^\infty e^{i\omega t} dt \, \langle n | j_\nu(0) | n' \rangle \langle n' | e^{iHt} j_\mu(0) e^{-iHt} | n \rangle e^{-\beta E_n} \end{array} \right] \\
&= \frac{i}{\omega Z} \sum_{nn'} \langle n | j_\mu(0) | n' \rangle \langle n' | j_\nu(0) | n \rangle \frac{e^{-\beta E_n} - e^{-\beta E_{n'}}}{\omega + E_n - E_{n'} + i\delta}
\end{aligned}
$$

where Z is the partition function $Z = \sum_n e^{-\beta E_n}, \beta = \frac{1}{k_B T}, T$ is temperature. For $T = 0, \beta \to \infty$, for $n = 0, E_0 = 0, e^{-\beta E_0} = 1$, for $n \neq 0, E_n > 0, e^{-\beta E_n} = 0$. The optical conductivity is simplified as

$$
\sigma_{\mu\nu}^{reg}(\omega) = \frac{i}{\omega} \sum_n \langle 0 | j_\mu(0) | n \rangle \langle n | j_\nu(0) | 0 \rangle \frac{1}{\omega + E_0 - E_n + i\delta}. \tag{B.2}
$$

Here $|0\rangle$ is the ground state $|\Psi_0\rangle$, and we consider the case $\mu = \nu$; then $j_\mu(0) = j_\nu(0) = J$, and the optical conductivity becomes

$$
\sigma^{reg}(\omega) = \frac{i}{\omega} \langle \Psi_0 | J \frac{1}{\omega + E_0 - H + i\delta} J | \Psi_0 \rangle. \tag{B.3}
$$

To evaluate this function, we choose the initial state to be $|\phi_0\rangle = \frac{J|\Psi_0\rangle}{\sqrt{\langle \Psi_0 | J^+ J | \Psi_0 \rangle}}$, then apply the Hamiltonian H to $|\phi_0\rangle$ many times to construct the Lanczos basis $|\phi_n\rangle$,

in this basis,

$$z - H = \begin{bmatrix} z - a_0 & -b_1 & 0 & 0 & ... \\ -b_1 & z - a_1 & -b_2 & 0 & ... \\ 0 & -b_2 & z - a_2 & -b_3 & ... \\ 0 & 0 & -b_3 & z - a_3 & ... \\ ... & ... & ... & ... & ... \end{bmatrix}$$

where $z = \omega + E_0 + i\delta, a_n, b_n$ are obtained by the same Lanczos procedure with the initial state $|\phi_0\rangle$. Consider the identity $(z - H)(z - H)^{-1} = I$ and expand it in the new basis $|\phi_0\rangle, ... |\phi_n\rangle$; we have

$$\sum_n \langle\phi_m|(z - H)|\phi_n\rangle\langle\phi_n|(z - H)^{-1}|\phi_q\rangle = \delta_{mq}. \tag{B.4}$$

Since we are interested in $\langle\phi_0|(z - H)^{-1}|\phi_0\rangle$, so let $q = 0, x_n = \langle\phi_n|(z - H)^{-1}|\phi_0\rangle$, and

$$\sum_n \langle\phi_m|(z - H)|\phi_n\rangle x_n = \delta_{m0}. \tag{B.5}$$

This becomes a system of equations for the unknown vector $\mathbf{X} = (x_0, x_1, x_2, ...x_n)^T$,

$$A\mathbf{X} = b$$

where A is a matrix with its elements given by $A_{mn} = \langle\phi_m|(z - H)|\phi_n\rangle$, and $b = (1, 0, 0, ...0)^T$. According to Cramer's rule, if the matrix A has a nonzero determinant, then the system has a unique solution

$$x_i = \frac{\det A_i}{\det A}$$

where A_i is obtained from A by replacing the nth column of A with b, specifically

$$
A_0 = \begin{bmatrix}
1 & -b_1 & 0 & 0 & \dots \\
0 & z-a_1 & -b_2 & 0 & \dots \\
0 & -b_2 & z-a_2 & -b_3 & \dots \\
0 & 0 & -b_3 & z-a_3 & \dots \\
\dots & \dots & \dots & \dots & \dots
\end{bmatrix}.
$$

The determinant of these matrices can be expanded as $\det A = \det(z - H) = (z - a_0)\det D_1 - b_1^2 \det D_2$, and $\det A_0 = \det D_1$, where D_n is obtained from $z - H$ by removing the first n rows and columns.

$$
\begin{aligned}
x_0 &= \frac{1}{(z-a_0) - b_1^2 \frac{\det D_2}{\det D_1}} \\
&= \frac{1}{(z-a_0) - \dfrac{b_1^2}{(z-a_1) - b_2^2 \frac{\det D_3}{\det D_2}}} \\
&= \frac{1}{(z-a_0) - \dfrac{b_1^2}{(z-a_1) - \dfrac{b_2^2}{(z-a_2) - \dots}}}.
\end{aligned}
$$

Then the optical conductivity at zero temperature is given by

$$
\sigma^{reg}(\omega) = \frac{i}{\omega} \frac{\langle \Psi_0 | J^+ J | \Psi_0 \rangle}{(z-a_0) - \dfrac{b_1^2}{(z-a_1) - \dfrac{b_2^2}{(z-a_2) - \dots}}}. \tag{B.6}
$$

Note that $z = \omega + E_0 + i\delta$, and once the ground state E_0 is known, we can calculate the spectral properties (optical conductivity) accurately for any given frequency ω and width δ. To calculate the optical conductivity by the Lanczos method, we need to run the Lanczos subroutine twice. In the first run, we get the ground state energy E_0 and wavefunction $|\Psi_0\rangle$. In the second run, we take $J|\Psi_0\rangle$ as the initial state and

obtain a_n and b_n by the Lanczos procedure.

APPENDIX C

Notes for Chapter 3

C.1 Density of states at the bottom of the band

Expanding $\varepsilon_{k,-}$ around the minimum energy E_0, by defining $k_x' = k_x \pm \arctan(\frac{V_S}{\sqrt{2}t})$, $k_y' = k_y \pm \arctan(\frac{V_S}{\sqrt{2}t})$, we have

$$\varepsilon_{k,-} - E_0 = \frac{0.5t}{\sqrt{1 + V_S^2/(2t^2)}}[(1 + V_S^2/t^2)(k_x'^2 + k_y'^2) \pm 2k_x'k_y'] \qquad \text{(C.1)}$$

To calculate the density of states at the bottom of the band, from the definition, we have

$$D_-(E_0 + E_1) = \frac{1}{4\pi^2} \int_{-\pi}^{\pi} dk_x \int_{-\pi}^{\pi} dk_y \delta(E_0 + E_1 - \varepsilon_{k,-}), \qquad \text{(C.2)}$$

where E_1 is a small amount of energy above the bottom of the band, E_0. Around the four energy minimum points there are four small regions which will contribute to this integral. We choose one of them (and then times our results by a factor of 4) and use the definitions of k' above instead of k, introduce a small cutoff k_c which

is the radius of a small circle around $k_{\min}$, thus the integral reads

$$
\begin{aligned}
D_-(E_0 + E_1) &= 4 \times \frac{1}{4\pi^2} \int_0^{k_c} k' dk' \int_{-\pi}^{\pi} d\theta \\
&\times \delta\left(E_1 - \frac{0.5t}{\sqrt{1 + V_S^2/(2t^2)}}[(1 + V_S^2/t^2) + \sin 2\theta]k'^2\right) \\
&= \frac{\sqrt{1 + V_S^2/(2t^2)}}{\pi^2 t} \int_{-\pi}^{\pi} d\theta \frac{1}{[(1 + V_S^2/t^2) + \sin 2\theta]} \\
&= \frac{\sqrt{2}}{\pi} \frac{1}{V_S}.
\end{aligned} \tag{C.3}
$$

The derivation of the effective mass in the weak coupling approximation (Eq. (3.20)) proceeds similarly. We begin with Eq. (D.4) in the text for the self energy. For very small phonon frequency we need only focus on the lower Rashba band, $s = -1$. Furthermore, the non-interacting electron energy can be expanded about a minimum, as in Eq. (C.1). Noting that there are four equal contributions coming from the four degenerate minima, we obtain

$$
\Sigma_{\text{weak}}(\omega + i\delta) = -4 \frac{\pi \lambda t \omega_E}{(2\pi)^2} \int dk'_x \int dk'_y
$$
$$
\frac{1}{a^2 + \frac{t}{2\sqrt{1 + \frac{V_S^2}{2t^2}}}\left[(1 + (V_S/t)^2)(k'^2_x + k'^2_y) + 2k'_x k'_y\right]} \tag{C.4}
$$

where $a^2 = E_0 + \omega_E - \omega$, and the integration is understood to be around a small disk located at one of the energy minima. Transforming to polar coordinates allows both the radial and angular integral to be done analytically; for the radial integral we keep only the dominant portion for small ω_E, and, after differentiation, we readily obtain the result quoted in the text (Eq. (3.20)).

C.2   Strong coupling limit

To investigate the strong coupling limit using second order perturbation, we need to evaluate Eq. (3.15), repeated here for convenience:

$$
E_{k-}^{(2)} = \sum_{n_{TOT} \neq 0, n1, n2, \ldots = 0, 1, \ldots \infty} \sum_{\substack{\ell = 1 \\ \sigma}}^{N}
$$

$$
\frac{\left| \langle n_1, n_2, \ldots n_N |_{ph} \otimes \langle c_{\ell\sigma}|_{el} \overline{T} |\Psi_{k,-}\rangle_{el} \otimes |0\rangle_{ph} \right|^2}{-n_{TOT}\omega_E}
$$

$$
= \frac{-t^2 e^{-2g^2}}{\omega_E} \sum_{\substack{n1, n2.. = 0 \\ n_{\mathrm{TOT}} \neq 0}}^{\infty} \sum_{\ell = 1}^{N} \frac{|A_\uparrow|^2 + |A_\downarrow|^2}{n_{\mathrm{TOT}}}, \tag{C.5}
$$

where A_σ is given a series of matrix elements (distinct for $\sigma = \uparrow$ and $\downarrow$). These turn out to give equal contributions, so we illustrate in some detail the result for $A_\uparrow$ only. After some algebra, we obtain

$$
|A_\uparrow|^2 = |u_\ell(-g)|^2 \; | \sum_{\delta = \pm x, \pm y} c_\delta u_{\ell+\delta}(g)|^2, \tag{C.6}
$$

where

$$
u_\ell(\pm g) \equiv \langle n_\ell | e^{\pm g a_\ell^\dagger} |0\rangle = \frac{(\pm g)^{n_\ell}}{\sqrt{n_\ell!}} \tag{C.7}
$$

and

$$
\begin{aligned}
c_{+x} &= e^{+ik_x a}\Big(1 + \frac{V_S}{t}e^{i\phi_k}\Big) \\
c_{-x} &= e^{-ik_x a}\Big(1 - \frac{V_S}{t}e^{i\phi_k}\Big) \\
c_{+y} &= e^{+ik_y a}\Big(1 - i\frac{V_S}{t}e^{i\phi_k}\Big) \\
c_{-y} &= e^{-ik_y a}\Big(1 + i\frac{V_S}{t}e^{i\phi_k}\Big),
\end{aligned} \tag{C.8}
$$

and

$$e^{i\phi_k} \equiv \frac{\sin{(k_y a)} - i\sin{(k_x a)}}{\sqrt{\sin^2{(k_x a)} + \sin^2{(k_y a)}}}. \tag{C.9}$$

For each of the $u_\ell(\pm g)$ in Eq. (C.6) it is to be understood that $n_\ell \neq 0$, but all other $n_{\ell'} = 0$ for $\ell' \neq \ell$. Hence, in the 16 terms in Eq. (C.6), 12 will have all phonon numbers equal to zero (other than n_ℓ); the other 4 will have both n_ℓ and $n_{\ell+x}$ (or n_ℓ and $n_{\ell-x}$, etc.) not equal to zero in general. As already mentioned, the contribution from $|A_\downarrow|^2$ is identical to that from $|A_\uparrow|^2$, so this merely gives us a factor of 2 in Eq. (C.5). Moreover, translational invariance makes the contribution from each site identical, so the sum over sites is trivially performed. This equation then becomes

$$E_{k-}^{(2)} = -\frac{4t^2 e^{-2g^2}}{\omega_E}\{f(g^2)\left(\frac{\epsilon_{k-}}{2t}\right)^2 + \left[f(2g^2) - f(g^2)\right]\left[1 + \left(\frac{V_S}{t}\right)^2\right]\}, \tag{C.10}$$

where

$$\begin{aligned} f(x) &\equiv \sum_{n=1}^{\infty}\frac{1}{n}\frac{x^n}{n!} = Ei(x) - \gamma - \ln x \\ &\approx e^x/x\left[1 + 1/x + 2/x^2 + ...\right], \end{aligned} \tag{C.11}$$

and $Ei(x)$ is the exponential integral and $\gamma \approx 0.5772$ is Euler's constant. Eq. (C.10) leads directly to Eq. (D.8) in the text.

APPENDIX D

Notes for Chapter 4

D.1 Density of States and effective mass

Expanding $\varepsilon_{k,-}$ around the minimum energy E_0, by defining $k'_x = k_x \pm \arctan(\frac{V_R+V_D}{\sqrt{2}t})$, $k'_y = k_y \pm \arctan(\frac{V_R+V_D}{\sqrt{2}t})$, we have

$$\varepsilon_{k,-} - E_0 = \widetilde{t_1}(k'^2_x + k'^2_y) \pm \widetilde{t_2}k'_x k'_y \tag{D.1}$$

where $\widetilde{t_1} = \dfrac{t[1+\frac{(V_R+V_D)^2}{2t^2}-\frac{(V_R-V_D)^2}{2(V_R+V_D)^2}]}{\sqrt{1+(V_R+V_D)^2/(2t^2)}}$ and $\widetilde{t_2} = \dfrac{t\frac{(V_R-V_D)^2}{(V_R+V_D)^2}}{\sqrt{1+(V_R+V_D)^2/(2t^2)}}$. To calculate the density of states at the bottom of the band, from the definition, we have

$$D_-(E_0 + E_1) = \frac{1}{4\pi^2} \int_{-\pi}^{\pi} dk_x \int_{-\pi}^{\pi} dk_y \delta(E_0 + E_1 - \varepsilon_{k,-}), \tag{D.2}$$

where E_1 is a small amount of energy above the bottom of the band, E_0. Around the two energy minimum points there are two small regions which will contribute to this integral. We choose one of them (and then multiply our results by a factor of 2) and use the definitions of k' above instead of k, introduce a small cutoff k_c which

is the radius of a small circle around $k_{\min}$, thus the integral reads

$$
\begin{aligned}
D_-(E_0 + E_1) &= 2 \times \frac{1}{4\pi^2} \int_0^{k_c} k' dk' \int_{-\pi}^{\pi} d\theta \\
&\times \delta(E_1 - [\widetilde{t_1} + \frac{1}{2}\widetilde{t_2}\sin 2\theta]k'^2) \\
&= \frac{1}{2\pi t} \frac{1}{\sqrt{1 + \frac{(V_R+V_D)^2}{2t^2} - \frac{(V_R-V_D)^2}{(V_R+V_D)^2}}}
\end{aligned}
\tag{D.3}
$$

In the weak electron-phonon coupling regime, perturbation theory can be applied to evaluate the effective mass, the self energy to first order in λ is given by

$$
\Sigma_{\text{weak}}(\omega + i\delta) = \pi\lambda t\omega_E \sum_{\mathbf{k},s=\pm} \frac{1}{\omega + i\delta - \omega_E - \varepsilon_{k,s}}.
\tag{D.4}
$$

The effective mass can be obtained by the derivative of the self energy

$$
\frac{m^*_{\text{weak}}}{m_{SO}} = 1 - \frac{\partial}{\partial\omega}\Sigma_{\text{weak}}(\omega + i\delta)|_{\omega=E_0}.
\tag{D.5}
$$

By inserting the expansion of $\varepsilon_{k,-}$ around the minimum energy E_0 into Eqn.[D.4] and Eqn.[D.5], we are ready to obtain the effective mass near the adiabatic limit as

$$
\frac{m^*_{\text{weak}}}{m_{SO}} = 1 + \frac{\lambda}{2} \frac{1}{\sqrt{1 + \frac{(V_R+V_D)^2}{2t^2} - \frac{(V_R-V_D)^2}{(V_R+V_D)^2}}}.
\tag{D.6}
$$

The effective mass has a minimum for $V_R = V_D$ while $V_R + V_D$ is a constant.

D.2 Strong coupling theory

To investigate the strong coupling regime of the Rashba-Dresselhaus-Holstein model for a single polaron, we use the Lang-Firsov (Lang and Firsov, 1963; Marsiglio, 1995) unitary transformation $\overline{H} = e^S H e^{-S}$, where $S = g\sum_{i,\sigma} n_{i,\sigma}(a_i - a_i^\dagger)$. Following

similar procedures to those in Li et al. (2011), we obtain the first order perturbation correction to the energy as

$$E_{k\pm}^{(1)} = e^{-g^2}\varepsilon_{k\pm} - g^2\omega_E, \tag{D.7}$$

where g is the same band narrowing factor as obtained in the Holstein model. To find the second order correction to the ground state energy, we proceed as in Li et al. (2011), and find

$$
\begin{aligned}
E_{k-}^{(2)} &= -4e^{-2g^2}\frac{t^2 + (V_R)^2 + (V_D)^2}{\omega_E} \\
&\quad \times \left[f(2g^2) - f(g^2)\right] - e^{-2g^2}f(g^2)\frac{\epsilon_{k-}^2}{\omega_E},
\end{aligned}
\tag{D.8}
$$

where $f(x) \equiv \sum_{n=1}^{\infty} \frac{1}{n}\frac{x^n}{n!} \approx e^x/x\left[1 + 1/x + 2/x^2 + ...\right]$. Thus the ground state energy, excluding exponentially suppressed corrections, is

$$E_{GS} = -2\pi t\lambda\left(1 + 2\frac{t^2 + (V_R)^2 + (V_D)^2}{(2\pi t\lambda)^2}\right), \tag{D.9}$$

and there is a correction of order $1/\lambda^2$ compared to the zeroth order result. Corrections in the dispersion enter in strong coupling only with an exponential suppression. The ground state energy predicted by strong coupling theory has a maximum for $V_R = V_D$ while $V_R + V_D$ is a constant.

APPENDIX E

Notes for Chapter 5

E.1   Perturbation Theory

It is sometimes stated that for a momentum-independent self energy, the quasi-particle residue is equal to the inverse of the effective mass. This follows simply by comparing Eqs. (5.9) and (5.12). On the other hand, we have argued that Eq. (5.10) is more appropriate for the effective mass, in which case this statement appears not to be true. A resolution of this difficulty is straightforward for the Holstein model, which we outline below, but, interestingly, not possible for the BLF-SSH model, at least in one dimension. The essential difference appears to be that in the Holstein model the (phonon) excitations are gapped, whereas they are not in the BLF-SSH model because of the low-lying acoustic modes at small momentum transfer. In this appendix we focus attention on one dimension, where some subtleties arise.

For the Holstein model the computation of the self energy in weak coupling is

straightforward (Marsiglio, 1995). We obtain

$$\Sigma_H(\omega) = \frac{2t\omega_E\lambda_H\mathrm{sgn}(\omega - \omega_E)}{\sqrt{(\omega - \omega_E)^2 - (2t)^2}}. \tag{E.1}$$

The location of the quasiparticle pole at zero momentum (ground state) is then given by

$$\omega + 2t = -\frac{2t\omega_E\lambda_H}{\sqrt{(\omega - \omega_E)^2 - (2t)^2}}, \tag{E.2}$$

which can readily be determined numerically. Denoting the solution by writing $\omega \equiv -2t - E_b$ (so E_b is the 'binding' energy below the bottom of the band), we can then use this in the spectral function, Eq. (5.11), to determine the residue z_0 in the quasiparticle peak at $\omega = E_b$:

$$A(k = 0, \omega) = z_0\delta(\omega + 2t + E_b) + \text{incoherent part}. \tag{E.3}$$

Straightforward calculation gives

$$z_0 = 1/\left(1 + \frac{2\lambda_H\tilde{\omega}_E\left[1 + 2\tilde{\omega}_E + 2\tilde{E}_b\right]}{\left[(1 + 2\tilde{\omega}_E + 2\tilde{E}_b)^2 - 1\right]^{3/2}}\right), \tag{E.4}$$

which is *not* in agreement with the inverse of Eq. (5.22), except when λ_H is truly very small. Here $\tilde{E}_b \equiv E_b/(2t)$.

In particular, for arbitrarily small λ_H, $\partial\Sigma(\omega)/\partial\omega|_{\omega=-2t}$, which is used in Eq. (5.22), diverges as $\omega_E \to 0$, leading to a divergent effective mass (and therefore associated residue of zero). On the other hand, from Eq. (E.2) one readily sees

$$\lim_{\omega_E \to 0} E_b = t\big(\lambda\omega_E/t\big)^{2/3}, \tag{E.5}$$

from which Eq. (E.4) yields the result

$$\lim_{\omega_E \to 0} z_0 = 2/3, \tag{E.6}$$

surprisingly a universal number. The actual weight in the quasiparticle peak of the spectral function given by Eq. (5.11) for any given (even very small) value of λ_H actually tracks Eq. (E.4), and not the inverse of Eq. (5.22).

Interestingly, for the Holstein model, one can take a different tact towards calculating the spectral function: using perturbation theory to compute the perturbed wave function, which is then inserted into the calculation for the matrix elements required in the definition of the spectral function, one obtains

$$
\begin{aligned}
A_{\text{pert}}(k = 0, \omega \quad) \quad &= z_0^{\text{pert}} \delta(\omega + 2t + \frac{\lambda_H \omega_E}{\sqrt{(1 + 2\tilde{\omega}_E)^2) - 1}}) \\
&+ \quad \frac{1}{\pi} \frac{2t\omega_E \lambda_H}{(\omega + 2t)^2} \frac{\theta(2t - |\omega - \omega_E|)}{\sqrt{(2t)^2 - (\omega - \omega_E)^2}}.
\end{aligned} \tag{E.7}
$$

Note that there is no difficulty in integrating over this function, as the divergence in the denominator $(1/(\omega + 2t)^2)$ is not within (or bordering) the range of frequency given by the Heaviside function restriction in the numerator. This is due to the finite phonon frequency, ω_E. From this expression fulfillment of the sum rule determines that

$$z_0^{\text{pert}} = 1/\left(1 + \frac{2\lambda_H \tilde{\omega}_E [1 + 2\tilde{\omega}_E]}{[(1 + 2\tilde{\omega}_E)^2 - 1]^{3/2}}\right), \tag{E.8}$$

which *is in agreement* with the inverse of Eq. (5.22). The message is that, as long as we use the expression given by Eq. (5.11) for the spectral function, the area under the quasiparticle peak will correspond to Eq. (E.4), which is *not* the inverse of the effective mass, even if the self energy is independent of momentum.

In the BLF-SSH model, the self energy is evaluated numerically through Eq. (5.7).

An attempt to follow the procedure just outlined, which leads to Eqs. (E.7) and (E.8) for this model fails; this is because the phonon frequency goes to zero, so the restriction corresponding to the Heaviside function in Eq. (E.7) yields $-2t < \omega < 2t + \omega_0$; this in turn makes the divergence at $\omega = -2t$ non-integrable. One can only (in 1D) define the spectral function through Eq. (5.11), in which case the inverse of the effective mass differs from the quasiparticle pole for two reasons: the usual reason that the explicit momentum dependence now plays a role (see Eq. (5.10)), and, in addition, the derivative of the self energy with respect to frequency is evaluated at $\omega = -2t$ for the effective mass, whereas it is evaluated at the frequency corresponding to the pole for the quasiparticle residue.